

RL-TR-96-266
Final Technical Report
April 1997



EXTREMELY HIGH FREQUENCY DIRECTLY MODULATED LASERS

Cornell University

Robert Spencer, Joseph Greenberg, and Lester Eastman

APPROVED FOR PUBLIC RELEASE; DISTRIBUTION UNLIMITED.

19970605 096

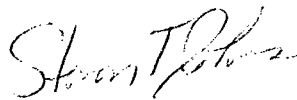
DTIC QUALITY INSPECTED 4

**Rome Laboratory
Air Force Materiel Command
Rome, New York**

This report has been reviewed by the Rome Laboratory Public Affairs Office (PA) and is releasable to the National Technical Information Service (NTIS). At NTIS it will be releasable to the general public, including foreign nations.

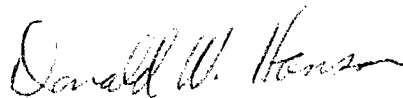
RL-TR-96-266 has been reviewed and is approved for publication.

APPROVED:



STEVEN T. JOHNS
Project Engineer

FOR THE COMMANDER:



DONALD W. HANSON, Director
Surveillance & Photonics Directorate

If your address has changed or if you wish to be removed from the Rome Laboratory mailing list, or if the addressee is no longer employed by your organization, please notify RL/OCPC, 25 Electronic Pky, Rome, NY 13441-4514. This will assist us in maintaining a current mailing list.

Do not return copies of this report unless contractual obligations or notices on a specific document require that it be returned.

REPORT DOCUMENTATION PAGE			Form Approved OMB No. 0704-0188	
Public reporting burden for this collection of information is estimated to average 1 hour per response, including the time for reviewing instructions, searching existing data sources, gathering and maintaining the data needed, and completing and reviewing the collection of information. Send comments regarding this burden estimate or any other aspect of this collection of information, including suggestions for reducing this burden, to Washington Headquarters Services, Directorate for Information Operations and Reports, 1215 Jefferson Davis Highway, Suite 1204, Arlington, VA 22202-4302, and to the Office of Management and Budget, Paperwork Reduction Project (0704-0188), Washington, DC 20503.				
1. AGENCY USE ONLY (Leave blank)		2. REPORT DATE April 1997	3. REPORT TYPE AND DATES COVERED FINAL, Sep 93 - Sep 96	
4. TITLE AND SUBTITLE EXTREMELY HIGH FREQUENCY DIRECTLY MODULATED LASERS			5. FUNDING NUMBERS C - F30602-93-C-0249 PE - 63726F PR - 2863 TA - 92 WU - 65	
6. AUTHOR(S) Robert Spencer, Joseph Greenberg, Lester Eastman				
7. PERFORMING ORGANIZATION NAME(S) AND ADDRESS(ES) Cornell University Office of Sponsored Programs 120 Day Hall Ithaca NY 14853			8. PERFORMING ORGANIZATION REPORT NUMBER	
9. SPONSORING / MONITORING AGENCY NAME(S) AND ADDRESS(ES) Rome Laboratory/OCPC 25 Electronic Pky Rome NY 13441-4515			10. SPONSORING / MONITORING AGENCY REPORT NUMBER RL-TR-96-266	
11. SUPPLEMENTARY NOTES Rome Laboratory Project Engineer: Steven T. Johns, OCPC, (315) 330-4456				
12a. DISTRIBUTION AVAILABILITY STATEMENT APPROVED FOR PUBLIC RELEASE; DISTRIBUTION UNLIMITED			12b. DISTRIBUTION CODE	
13. ABSTRACT (Maximum 200 words) Several novel directly modulated semiconductor laser structures have been investigated to increase the bandwidth of direct modulation. Detailed theoretical models were developed and a high-speed directly modulated laser was fabricated and tested. Corner reflector lasers that were compatible with monolithic integration were demonstrated to have the largest directly modulated bandwidth of any single sided output laser to date. The semiconductor laser tested produced a 20 GHz bandwidth. Theoretical and experimental results indicate that device heating was a major factor in limiting bandwidth of semiconductor lasers. Experiments utilizing flip-chip bonding semiconductor laser to diamond were conducted. These devices showed considerable improvements in both their DC and spectral behavior.				
14. SUBJECT TERMS InGaAs/A1GaAs MQW Laser, Diamond Heat Sinks, Directly Modulated Semiconductor Lasers			15. NUMBER OF PAGES 60	
			16. PRICE CODE	
17. SECURITY CLASSIFICATION OF REPORT UNCLASSIFIED	18. SECURITY CLASSIFICATION OF THIS PAGE UNCLASSIFIED	19. SECURITY CLASSIFICATION OF ABSTRACT UNCLASSIFIED	20. LIMITATION OF ABSTRACT UNLIMITED	

Extremely High Frequency Directly Modulated Lasers

Principle Investigator: Professor Lester F. Eastman

Senior Research Associate: William J. Schaff

Visiting scientists: Alex Tager, Professor Brian Ridley

Graduate students: Bradley Foreman, Joseph Greenberg, Trung Letran, Sean O'Keefe, Robert
Spencer, Chin-Yi Tsai

Cornell University, Ithaca, NY 14853

1. ABSTRACT.....	2
2. PUBLICATIONS AND PRESENTATIONS.....	3
3. OUTLINE.....	8
4. OPTIMIZATION AND MATERIAL DESIGN.....	10
5. CORNER REFLECTOR LASERS.....	13
6. DIAMOND HEAT SINKS.....	25
7. CARRIER HEATING AND CARRIER TRANSPORT.....	38
8. (111)-ORIENTED LASERS.....	44
9. SUMMARY AND FUTURE WORK.....	49
10. REFERENCES.....	51

ABSTRACT

The EHF Directly Modulated Laser project was undertaken to develop optical sources that would be able to superimpose a microwave signal at 44 GHz onto an optical carrier at 1.3 μm . The theoretical limitations on the directly modulated bandwidths of semiconductor lasers were investigated to explain the observed limitations on their performance. Detailed theoretical models were developed that for the first time included the effects of carrier diffusion, capture, escape, and heating. The results of these models not only verified experimental results that had previously been unexplained, but aided in designing optimized structures for high speed performance. An analytical density of states formula was derived to aid in the modeling of semiconductor lasers.

With theoretical and experimental results both indicating that device heating was a major factor in limiting the bandwidth of semiconductor lasers, we sought to improve the heat sinking of these devices by flip-chip bonding them to diamond. CPW lines were fabricated on CVD diamond and cleaved facet devices were successfully bonded. These devices showed a marked improvement in both their DC and spectral behavior.

Several novel structures to improve the bandwidth of semiconductor lasers were investigated. Corner reflector lasers that were compatible with monolithic integration were designed, fabricated and tested. These devices have demonstrated the largest directly modulated bandwidth of any single-sided output laser yet produced. (111)-oriented lasers were investigated for the possibility of achieving 1.3 μm wavelengths in a GaAs-based device, and, thereby, opening the much higher bandwidths achieved in this material system to the this longer wavelength. We found that such devices can not only reach 1.3 μm , but that they are technologically feasible and may outperform current state-of-the-art InP-based laser diodes.

PUBLICATIONS AND PRESENTATIONS

Papers written with the support of this contract:

“Hot carrier and hot phonon effects in high-speed quantum well lasers”, C. Y. Tsai, L. F. Eastman, and Y. H. Lo, *Appl. Phys. Lett.*, vol. 63, n. 25, pp. 3408-3410, 1993.

“Effective-mass Hamiltonian and boundary conditions for the valence bands of semiconductor microstructures”, B. A. Foreman, *Phys. Rev. B* vol. 48, n. 7, pp. 4964-4967, 1993.

“Space-charge-mediated capture of electrons and holes in a quantum well”, B. K. Ridley, *Phys. Rev. B*, vol. 50, n. 3, pp. 1717-1724, 1994

“Carrier energy relaxation in multisubband quantum well lasers with hot phonon effects”, C. Y. Tsai, L. F. Eastman, Y. H. Lo, and C. Y. Tsai, *J. Appl. Phys.*, vol. 76, n. 9, pp. 5334-5338, 1994.

“Carrier capture and escape in multisubband quantum well lasers”, C. Y. Tsai, L. F. Eastman, Y. H. Lo, and C. Y. Tsai, *IEEE Photon. Technol. Lett.*, vol. 6, n. 9, pp. 1088-1090, 1994.

“Breakdown of thermionic emission theory for quantum wells”, C. Y. Tsai, L. F. Eastman, Y. H. Lo, and C. Y. Tsai, *Appl. Phys. Lett.*, vol. 65, n. 4, pp. 469-471, 1994.

“Analytic model for the valence-band structure of a strained quantum well”, B.A. Foreman, *Phys. Rev. B*, vol. 49, n. 3, pp. 1757-1773, 1994.

“Foundations of the envelope-function theory for phonons in polar semiconductor heterostructures”, B.A. Foreman, *22nd International Conference on the Physics of Semiconductors*, vol. 2, p. 911-914, 1994

“Microwave Characterization of Corner Reflector p-Doped Multiple Quantum-Well Lasers”, R.M. Spencer, S.S. O’Keefe, G.H. Martin, W.J. Schaff, and L.F. Eastman, *IEEE Photon. Technol. Lett.*, vol. 7, n. 1, pp. 20-22, 1995

“Temperature Effects on the High Speed Performance of Quantum Well Lasers”, Robert M. Spencer, Sean S. O’Keefe, William J. Schaff, Chin Y. Tsai, and Lester F. Eastman, *LEOS ‘95. IEEE Lasers and Electro-Optics Society 1995 Annual Meeting. 8th Annual Meeting. Conference Proceedings*, vol. 1, pp. 99-100, 1995

“Optical phonons in a quantum well containing monolayers”, B.K. Ridley, *Appl. Phys. Lett.*, vol. 66, n. 26, pp. 3633-3635, 1995

“Degradation of resonant frequency in high-speed quantum well lasers: effects of spectral hole burning, hot carrier, hot phonon, and carrier diffusion-capture-escape”, Chin-Yi Tsai, Yu-Hwa Lo, Robert M. Spencer, Lester F. Eastman, and Chin-Yao Tsai, *LEOS ‘95. IEEE Lasers and Electro-Optics Society 1995 Annual Meeting. 8th Annual Meeting. Conference Proceedings*, vol. 1, pp. 97-98, 1995

“Effects of Spectral Hole Burning, Carrier Heating, and Carrier Transport on the Small-Signal Modulation Response of Quantum Well Lasers”, Chin-Yi Tsai, Chin-Yao Tsai, Yu-Hwa Lo, R.M. Spencer, *Appl. Phys. Lett.*, vol. 67, n. 21, pp. 3084-3086, 1995

“Effects of hot phonons on carrier heating in quantum-well lasers”, C.Y. Tsai, Y.H. Lo, R.M. Spencer, and C.Y. Tsai, *IEEE Photon. Technol. Lett.*, vol. 7, n. 9, pp. 950-952, 1995

“Nonlinear Gain Coefficients in Semiconductor Quantum Well Lasers: Effects of Carrier Diffusion, Capture, and Escape”, C.Y. Tsai, Y.H. Lo, R.M. Spencer, L.F. Eastman, *IEEE J. Select. Topics on Quantum Electron.*, vol. 1, n. 2, pp. 316-330, 1995

“Optimization of the optical guide design and cavity design of multiple quantum well lasers for efficient microwave optical links”, R.M. Spencer, S.S. O’Keefe, C.Y. Tsai, J. Greenberg, J. Braunstein, G.H. Martin, W.J. Schaff, and L.F. Eastman , *Proceeding of the 1995 15th Biennial IEEE/Cornell University Conference on Advanced Concepts in High Speed Semiconductor Devices and Circuits*, pp. 152-159, 1995

“Side-mode suppression for long DBR lasers”, Alexei A. Tager, *IEEE Photon. Technol. Lett.*, vol. 7, n. 8, pp. 866-868

“A Theoretical Investigation on the Effects of Spectral Hole Burning, Hot Carrier, Hot Phonon and Carrier Diffusion-Capture-Escape on the limitations of the Modulation Bandwidth in High-Speed Quantum Well Lasers”, C.Y Tsai, Y.H. Lo, R. M. Spencer, and L.F. Eastman, *Proceedings of the 1995 15th Biennial IEEE/Cornell University Conference on Advanced Concepts in High Speed Semiconductor Devices and Circuits*, pp. 415-424, 1995

“Carrier DC and AC capture and escape times in quantum well lasers”, C.Y. Tsai, C.Y. Tsai, Y.H. Lo, and L.F. Eastman, *IEEE Photon. Technol. Lett.*, vol. 7, n. 6, pp. 599-601, 1995.

“Exact effective-mass theory for heterostructures”, B.A. Foreman, *Phys. Rev. B*, vol. 52, n. 16, pp.12241-12259, 1995

“Foundations of the envelope-function theory for phonons in heterostructures”, B.A. Foreman, *Phys. Rev. B*, vol. 52, n. 16, pp. 12260-12281, 1995

“Carrier energy relaxation time in quantum-well lasers”, Chin-Yi Tsai, Chin-Yao Tsai, Yu-Hwa Lo, and L.F. Eastman, *IEEE J. of Quant. Electron.*, vol. 31, n. 12, pp. 2148-2158, 1995

“Optimization of semiconductor lasers for UHF modulation”, Lester Eastman and Robert Spencer, *Proc. SPIE - Int. Soc. Opt. Eng. (USA), Proceedings of the SPIE - The International Society for Optical Engineering*, vol. 2693, pp. 406-417, 1996

“Nonlinear Gain Coefficients in Semiconductor Lasers: Effects of Carrier Heating”, Chin-Yi Tsai, Chin-Yao Tsai, Robert Spencer, Yu-Hwa Lo, and Lester F. Eastman, *IEEE J. Quantum Electron.*, vol. 32, no. 2, pp. 201-212, 1996.

“High-speed direct modulation of semiconductor lasers”, Robert M. Spencer, Joseph Greenberg, Lester F. Eastman, Chin-Yi Tsai, Sean S. O’Keefe, *Int. J. of High Speed Electron. and Systems*, in press

“A novel structure incorporating ordered $(\text{InAs})_1(\text{GaAs})_1$ quantum wells on GaAs(111)B for high speed long wavelength lasers up to and beyond $1.3\ \mu\text{m}$ ”, Joseph Greenberg, and Lester F. Eastman, *Proceedings of the 23rd International Symposium on Compound Semiconductors*, St. Petersburg, Russia, September 23-27, 1996, in press

“ $1.3\ \mu\text{m}$ lasers on GaAs(111)B employing ordered $(\text{InAs})_1(\text{GaAs})_1$ quantum wells for high frequency response applications”, Joseph Greenberg, and Lester F. Eastman, *Microelectronics Journal*, in press

Conference presentations

“Strained multi-quantum-well lasers for high frequency modulation”, Lester F. Eastman, (Invited) DOD Fiber Optics and Photonics Conference, McLean, VA, March 22-25, 1994

“Optoelectronic devices for high frequency operation”, Lester F. Eastman, (Invited) IEEE Rome/Utica Meeting, May 23-26, 1994

“Microwave Response of Corner Reflector Lasers”, R.M. Spencer, S.S. O’Keefe, G.H. Martin, W.J. Schaff, and L.F. Eastman, presented at the *High Speed Optoelectronic Devices for Communication and Interconnects Conference*, San Luis Obispo, CA, August 14-18, 1994

“Temperature Effects on the Performance of High Speed Quantum Well Lasers”, R.M. Spencer, S. S. O’Keefe, C.Y. Tsai, J. Greenberg, J. Braunstein, G.H. Martin, W.J. Schaff, and L.F. Eastman, presented at the *19th Workshop on Compound Semiconductor Devices and Integrated Circuits*, Stockholm, Sweden, May 21-24, 1995

Dissertations supported and partially supported by this contract

C. Y. Tsai, *Particle Dynamics and Energy Transfer in High-Speed Quantum Well Lasers: Effects of Spectral Hole Burning, Carrier Heating, and Carrier Transport*. Ph.D. dissertation, Cornell University, Ithaca, NY, 1995

B.A. Foreman, *Foundations of the envelope-function theory for electrons and phonons in semiconductor heterostructures*, Ph.D. dissertation, Cornell University, Ithaca, NY, 1995

S.S. O’Keefe, *Design, growth, fabrication, and characterization of vertical cavity surface emitting lasers flip chip bonded to microwave compatible diamond heat sinks*, Ph.D. dissertation, Cornell University, Ithaca, NY, 1996

R.M. Spencer, *Technology and Theory of High-Frequency Directly Modulated Semiconductor Lasers*, Ph.D. dissertation, Cornell University, Ithaca, NY, 1997

OUTLINE

The overall goal for this project was to create optical sources that were capable of superimposing a microwave signal at 44 GHz onto an optical carrier at 1.3 μm . The method chosen to achieve this was to create a high speed directly modulated semiconductor laser with a bandwidth of 44 GHz.

To accomplish this goal, the project was subdivided as follows:

- I. Explore the physics and technology of directly modulated lasers using the well-known InGaAs-GaAs material system.
 - A. Explore novel material designs for large bandwidth lasers.
 - B. Experimentally determine the limitations on directly modulated semiconductor lasers
 - C. Design, fabricate, and test novel laser cavity structures, such as the corner reflector laser
 - D. Design, fabricate, and test lasers flip-chip mounted onto diamond heat sinks to reduce the temperature rise in the active region at high input current levels
- II. Create broad bandwidth sources at the 1.3 μm wavelength
 - A. Optimize the design, growth, and characterization of InP based 1.3 μm lasers
 - I. Design, grow, and fabricate stress-compensated lasers using InGaAsP with MOCVD
 - ii. Design, grow, and fabricate 1.3 μm lasers using InAlGaAs grown by MBE
 - B. Explore novel methods for creating large bandwidth lasers at 1.3 μm
 - I. Lasers on (111) substrates

- ii. Lasers on ternary substrates

III. Create the analytical tools for understanding directly modulated semiconductor lasers

- A. Understand the theoretical limitations on directly modulating semiconductor lasers

- i. Effect of carrier heating and lattice heating

- ii. Effect of carrier transport

- B. Analytical density of states formula for the valence band

The remainder of this report will cover these topics in more detail. The final section will summarize our results and present our conclusions on the future of directly modulated lasers.

OPTIMIZATION AND MATERIAL DESIGN

Material design and analysis was done at Cornell using two methods. The first used an analytical density of states formula developed at Cornell to model the effect of an increase of the lattice temperature on the high-speed characteristics of semiconductor lasers. The second method used a fully numerical gain calculation program that was written by the University of California at Santa Barbara (UCSB) and transferred to Cornell via our relationship with UCSB within DARPA's Optoelectronic Technology Center (OTC). This gain calculation program numerically calculated the valence band structure and the transition strengths for every possible transition. The output from this program was incorporated into various programs developed in-house to calculate the various figures of merit for high-speed lasers. In addition, the output of the UCSB program was also used for a theoretical examination of the linewidth enhancement factor. A long wavelength version of this program was also delivered to Cornell for the design and analysis of InP based lasers.

Much of the design work in the area of ultra-high frequency directly modulated lasers was done at Cornell. However, many of the latest advances in the state of the art in semiconductor lasers have been done at the Fraunhofer-Institut für Angewandte Festkörperphysik (IAF) in Freiburg, Germany. These advances have come about due to an optimization of the material design that was not possible at Cornell because of monetary and manpower constraints. We have had a great deal of interaction with the IAF, and indeed many of their key people are products of our group and of Cornell. These include the lead scientist John Ralston (Cornell Eastman group graduate), the lead person in the microwave characterization group (Paul Tasker - a former senior research associate with the Eastman group), and the lead MBE scientist Eric Larkins (Cornell undergraduate). These persons and other member of the IAF staff have created the first semiconductor laser with a direct

modulation bandwidth of 40 GHz through a very exhaustive series of optimization trials. The most important of these optimization trials were in the area of MBE growth of strained quantum well lasers, with a majority of this work taking place at the IAF. Studies of the optimization of the growth temperature of InGaAs concluded that the ideal growth temperature of InGaAs was 500 °C, which is close to the indium desorption temperature. These studies led to high quality InGaAs multiple quantum well lasers with -3dB bandwidths of 20 GHz. Substantial improvements in the MBE growth of high-speed lasers were made by studying not only the InGaAs growth parameters, but also by examining the optimum growth conditions for the entire laser structure. It was found that optimizing the growth of the cladding layer was critical in improving device performance¹. Another significant milestone in the optimization of MBE growth parameters came with the introduction of short period superlattice (SPSL) cladding regions². A comparison of photoluminescence (PL) spectra from lasers grown with SPSL cladding regions and lasers grown with ternary cladding regions showed that the PL intensity from the SPSL lasers was five times stronger than the PL intensity from the ternary laser structures. In addition, low temperature cathodoluminescence topography showed regular 1-2 monolayer fluctuations in the QW widths of the ternary clad laser structures. These fluctuations were substantially reduced in the lasers with SPSL cladding regions. The growth of SPSL cladding layers, with As₂ provided by an arsenic cracker, allowed the substrate temperature to be reduced during the cladding growth. A comparison of two otherwise identical laser structures, one with the SPSL cladding grown at 700 °C, the other with the cladding grown at 620 °C, showed that the low temperature growth of the AlGaAs SPSL cladding greatly improved the laser performance. The threshold current densities were three times smaller, and the internal quantum efficiency improved from 60% to 70% for the lasers with cladding layers grown at 620 °C¹. The improved performance was attributed to the decrease of point defects within the MQW active regions which, in turn, reduced the formation of non-radiative recombination centers. Recently, lasers grown with SPSL cladding layers with the lower cladding grown at 700 °C and the upper cladding layer grown at 620°C produced the first

devices with a 40 GHz bandwidth³. Very low K-factors of 0.13 ns were obtained from lasers that are identical to the above mentioned 40 GHz devices but with p-type modulation doped active regions. The use of carbon for the p-type dopant improved the modulation doping characteristics of the active region. Previous work with Be as the p-type dopant showed that even though the Be was intended to be modulation doped, the Be diffused throughout the core region of the laser. Although these p-doped lasers have a very low K-factor, the -3dB bandwidth is limited to 37 GHz. The difference between the intrinsic bandwidth predicted by the K-factor (68 GHz) and the measured bandwidth of 37 GHz can perhaps best be explained by the lattice and carrier heating that takes place at large DC input currents. Nonetheless, the sheer amount of growth optimization that was necessary to produce these results was impressive. This type of sophistication is only available at a laboratory with the financial resources of the IAF, since the material, money, and manpower to perform the number of growth runs that were necessary are simply beyond the reach of any university.

There are a number of important results from the growth studies that were done at the IAF:

- (1) 40 GHz bandwidth semiconductor lasers *are* possible. There is nothing in the physics behind direct modulation that is preventing even larger bandwidths, both in short-wavelength lasers (GaAs based) and long-wavelength lasers.
- (2) The best lasers (at Cornell and the IAF) still have modulation responses that are underdamped, with the responses saturating well below their K-factor limit.
- (3) The most likely explanation for the saturation of the modulation bandwidth below the K-factor limit is the increase of the active region temperature with bias.

A more detailed understanding of the tradeoffs associated with both lattice and carrier heating will be necessary to improve the direct modulation bandwidth even further.

CORNER REFLECTOR LASERS

Most of the experimental research effort was directed toward understanding the ultimate limitations of directly modulated lasers on GaAs based substrates. The initial work performed was to explore the possibility of using a new type of laser, the corner reflector laser, in high speed optical communication links. The motivation for the corner reflector laser was to be able to demonstrate broad bandwidth, directly modulated lasers suitable for monolithic integration into OEICs. It was decided to fabricate lasers that had single-sided output to improve the total efficiency and to improve the threshold current characteristics. A corner reflector (CR) design that used total-internal-reflection (TIR) was used to provide a high-reflectivity facet. A p-doped strained MQW active region consisting of four $\text{In}_{0.3}\text{Ga}_{0.7}\text{As}/\text{Al}_{0.15}\text{Ga}_{0.85}\text{As}$ quantum wells was designed. The result of this project was the creation of the first broad bandwidth corner reflector lasers, with bandwidths of 20 GHz. The simple processing sequence for these devices, in conjunction with their single-sided output, makes these CR lasers attractive candidates for monolithic integration into OEICs. These lasers had K-factors near 0.1 ns, implying that their intrinsic bandwidth should be greater than 80 GHz. Lattice heating was the primary limitation on the bandwidth of these lasers.

Optical sources that are to be monolithically integrated alongside either other photonic elements or electronic circuits must have fabrication requirements compatible with these other photonic or electronic devices. In the case of semiconductor lasers, wafer level integration requires that the mirrors be fabricated with dry-etching since cleaved facets lasers are inherently incompatible with monolithic integration. In addition, for a number of applications, single-sided output is preferred over the standard dual output of lasers with two identical facets. Single-sided output avoids the necessity of ensuring that unwanted outputs do not interfere with other devices. It can also save GaAs chip real-estate since single-sided output lasers can be placed back-to-back without

interfering with each other. Because dry-etched mirrors must be used for devices that are suitable for monolithic integration, there is an advantage to being able to form a high-reflectivity mirror via the same process that creates the standard plane mirror. This can be done by etching a corner reflector for one facet and a standard plane mirror for the other facet, as shown in Figure 1. Compared to standard lasers with two plane mirrors, corner reflector lasers have previously demonstrated lower threshold currents, smaller far-field distributions, higher efficiencies, and they have been used to form phase-coupled arrays^{4,5,6,7}. It was decided to investigate the high-speed modulation of CR lasers to determine if the advantages previously reported for these lasers could also be extended to include broad bandwidth operation.

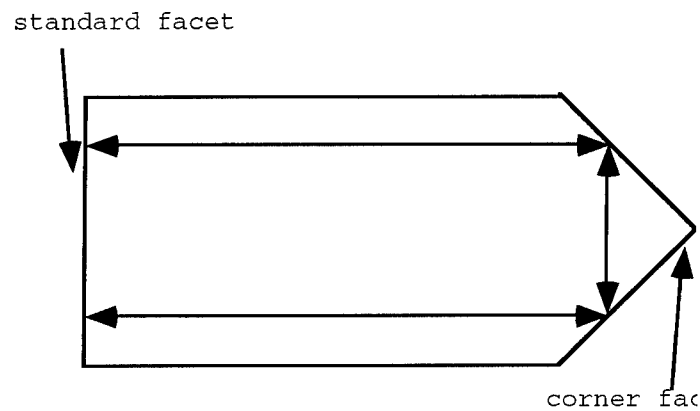


Figure 1: Top-down view of a corner reflector laser showing the total-internal-reflection at the corner facet.

Device structure

A four quantum well separate confinement heterostructure (SCH) laser was grown by molecular beam epitaxy (MBE) on a semi-insulating (SI) GaAs substrate. The optical guide was composed

of 50 Å $\text{In}_{0.3}\text{Ga}_{0.7}\text{As}$ wells separated by 170 Å $\text{Al}_{0.15}\text{Ga}_{0.85}\text{As}$ barriers with a total SCH width of 1800 Å. The laser structure that was grown consisted of: approximately 1 µm n+ GaAs ([Si] = $3 \times 10^{18} \text{ cm}^{-3}$) buffer, a lower 1500 Å n- $\text{Al}_x\text{Ga}_{1-x}\text{As}$ grading layer ($x=0 \Rightarrow 0.7$, [Si] = $4 \times 10^{18} \text{ cm}^{-3}$), an 8100 Å lower n-cladding layer ([Si] = $2 \times 10^{18} \text{ cm}^{-3}$) with 27 periods of $\text{Al}_{0.7}\text{Ga}_{0.3}\text{As}/\text{GaAs}$ (290 Å/10 Å), 400 Å of undoped $\text{Al}_{0.15}\text{Ga}_{0.85}\text{As}$, 145 Å of p-doped $\text{Al}_{0.15}\text{Ga}_{0.85}\text{As}$ ([Be] = $8 \times 10^{17} \text{ cm}^{-3}$), four 50 Å p-doped ([Be] = $8 \times 10^{17} \text{ cm}^{-3}$) $\text{In}_{0.3}\text{Ga}_{0.7}\text{As}$ quantum wells separated by 170 Å p-doped ([Be] = $8 \times 10^{17} \text{ cm}^{-3}$) $\text{Al}_{0.15}\text{Ga}_{0.85}\text{As}$ barriers, 575 Å of p-doped ([Be] = $8 \times 10^{17} \text{ cm}^{-3}$) $\text{Al}_{0.15}\text{Ga}_{0.85}\text{As}$, an 8100 Å upper p-cladding layer ([Be]

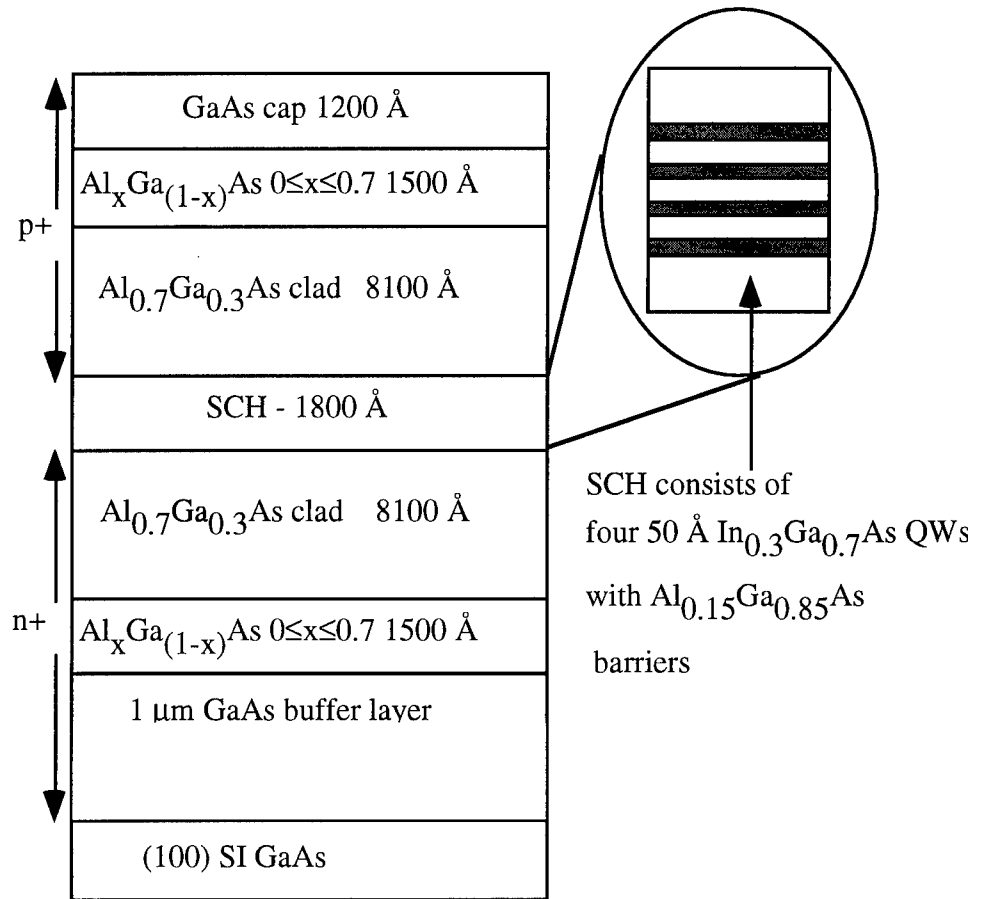


Figure 2: Wafer 4639 - SCH laser structure with four $\text{In}_{0.3}\text{Ga}_{0.7}\text{As}$ quantum wells.

$= 2 \times 10^{18} \text{ cm}^{-3}$) with 27 periods of $\text{Al}_{0.7}\text{Ga}_{0.3}\text{As}/\text{GaAs}$ (290 Å/10 Å), an upper 1500 Å p+ $\text{Al}_x\text{Ga}_{1-x}\text{As}$ grading layer ($x=0.7 \Rightarrow 0$, $[\text{Be}] = 3 \times 10^{19} \text{ cm}^{-3}$), and 1200 Å of p+ ($[\text{Be}] = 4 \times 10^{19} \text{ cm}^{-3}$) GaAs cap. The n+ buffer was grown at 580 °C, the upper and lower cladding layers were grown at 710 °C, the $\text{In}_{0.3}\text{Ga}_{0.7}\text{As}$ QWs were grown at 500 °C, the $\text{Al}_{0.15}\text{Ga}_{0.85}\text{As}$ barriers and optical guide material was grown at 620 °C, and the p+ GaAs cap layer was grown at 550 °C. A schematic of the laser structure is shown in Figure 2.

The p-type doping of the active region was implemented with uniform doping of the guide since it was felt that lack of control over the diffusion of the Be dopant due to the high temperature growth of the upper $\text{Al}_{0.7}\text{Ga}_{0.3}\text{As}$ cladding region would prevent successful modulation doping of the quantum wells. In addition, since uniform doping was used, the concentration was kept to just below $1 \times 10^{18} \text{ cm}^{-3}$ to minimize the internal loss factor of the laser.

The corner reflector laser processing sequence used chemically assisted ion beam etching (CAIBE) and a negative e-beam resist, SAL-601, as the etch mask. The process sequence is illustrated on the following page in Figure 3. After the material was grown, mesa lasers were fabricated in a geometry suitable for on-wafer microwave probing with coplanar waveguide (CPW) probes. Using standard lift-off techniques, a p-type metallization was deposited consisting of Ti/Pd/Au. The SAL-601 CAIBE mask was then patterned and the CAIBE etch was done to define the mirrors of the mesa to an etch depth of 2.3 µm. After mirror fabrication, n-type contacts of Ni/AuGe/Ag/Au were evaporated and annealed at 450 °C for 10 s, and devices were lapped and polished to 100 µm. A SEM photo and schematic of a corner reflector device is shown in Figure 4.

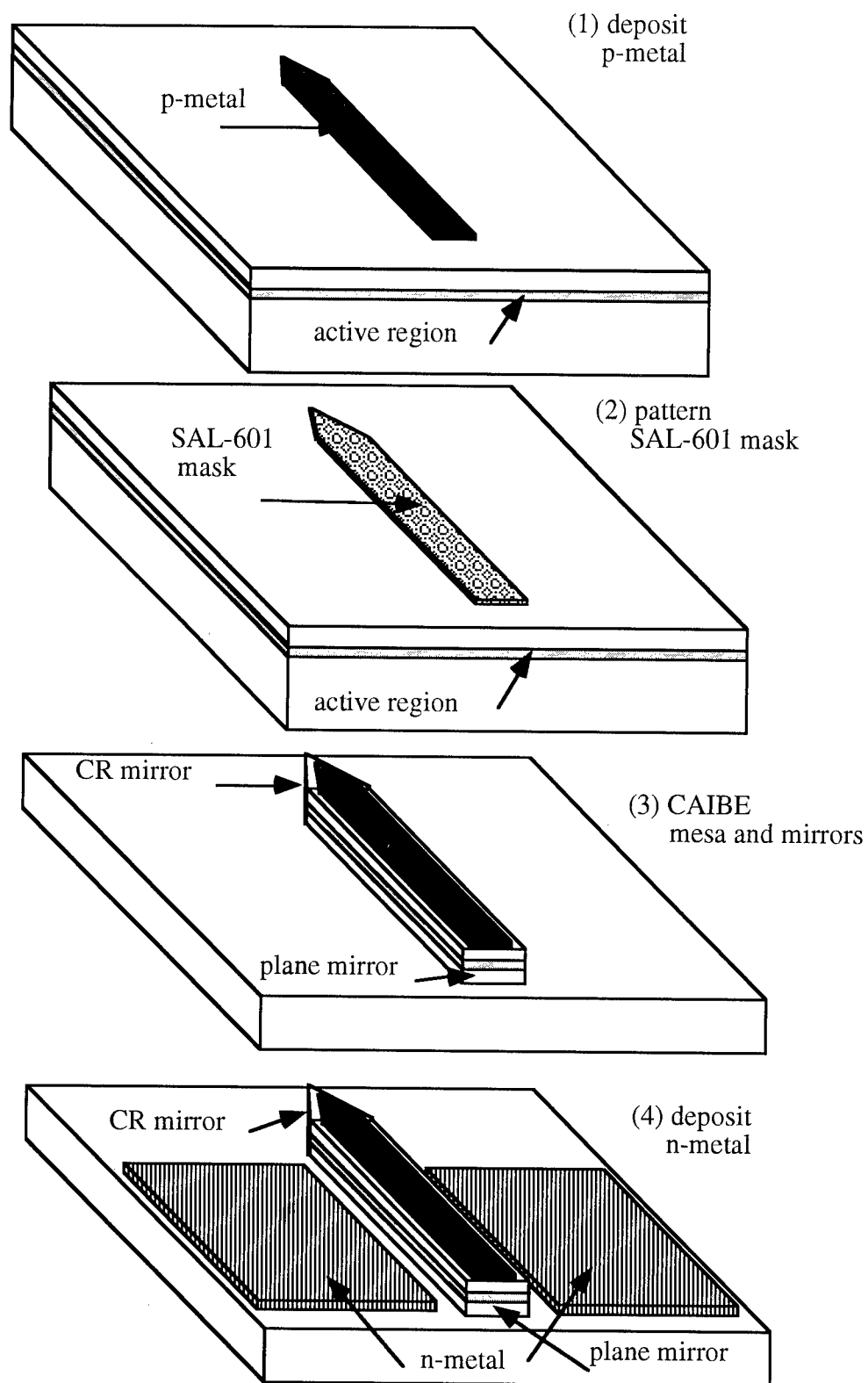


Figure 3: Process sequence for a corner reflector laser.

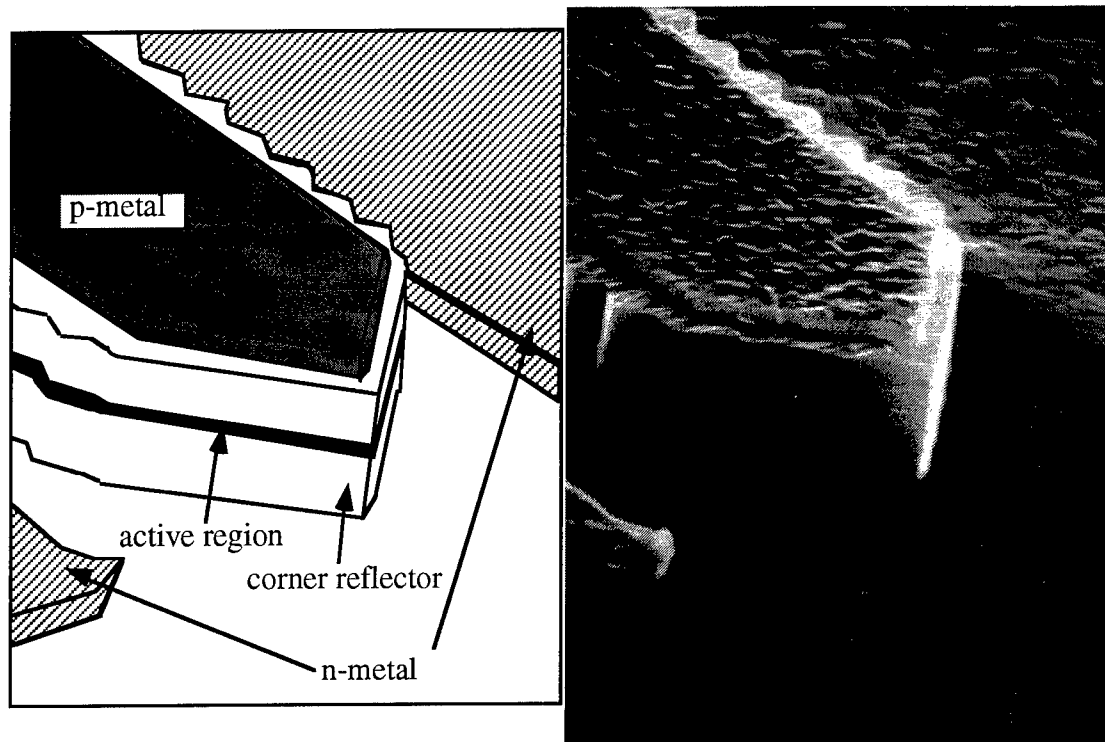


Figure 4: SEM and schematic showing the corner facet of a corner reflector laser.

The sides of the CR laser have been corrugated intentionally to make the mesa sidewalls non-reflective. This corrugation is especially important for lasers with two standard facets since a mesa geometry laser with four mirrors will not lase due to the circular modes that are possible in such a device.

In addition to CR lasers, devices with two plane mirror facets were fabricated. In both structures fabricated devices ranged in size from 100 μm to 400 μm . Once again, the Cambridge e-beam lithography tool was used for the entire process. Although the metallization steps could have easily been done with optical lithography, the e-beam tool was used for the convenience of not being required to make new masks for each change in the design layout.

The MBE growth of the laser was done in a Varian Gen II at Cornell by Sean O'Keefe. The growth methods used were developed by several researchers at Cornell and elsewhere.

The CW characterization was performed with a 4145A semiconductor parameter analyzer and UDT Si broad-area PIN diode detector. The UDT detector was factory calibrated and was placed immediately adjacent to the laser to capture the entire output. The first measurement performed was to test the effective unidirectional performance of the corner reflector laser by measuring the output from both facets. This PI measurement is shown in Figure 5. The output is essentially unidirectional, with a small amount of light output from the corner facet since the reflectivity is less than 100%. In addition, the threshold current for this device was 12 mA, which is lower than the 16 mA threshold current for standard lasers of the same size.

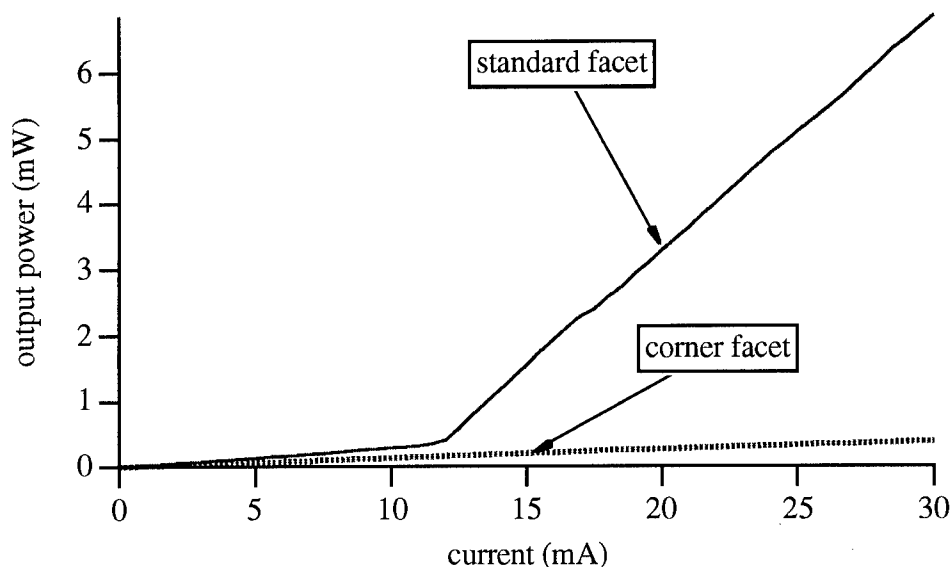


Figure 5: The output optical power as a function of input current at each facet of a corner reflector laser. The device size is $6\text{ }\mu\text{m} \times 150\text{ }\mu\text{m}$.

An approximate method for determining the mirror reflectivity of the corner facet is to measure the ratio of the output power from the standard and CR facets. The ratio of output power is given by⁸

$$\frac{P_s}{P_{CR}} = \left(\frac{R_{CR}}{R_s} \right)^{1/2} \left(\frac{1 - R_s}{1 - R_{CR}} \right)$$

where P_s (P_{CR}) is the output power of the standard (CR) facet, and R_s (R_{CR}) is the mirror reflectivity of the standard (CR) facet. To calculate the mirror reflectivity of the CR facet from Figure 5, the reflectivity of the standard dry-etched facet was assumed to be equal to the reflectivity of a cleaved facet ($R_s = 32\%$). Although this is not exactly true, comparisons between devices with two cleaved facets and two standard dry-etched facets have shown very similar threshold currents. The ratio of output power from the standard facet to the CR facet and the theoretical output power ratio are shown in Figure 6 and Figure 7.

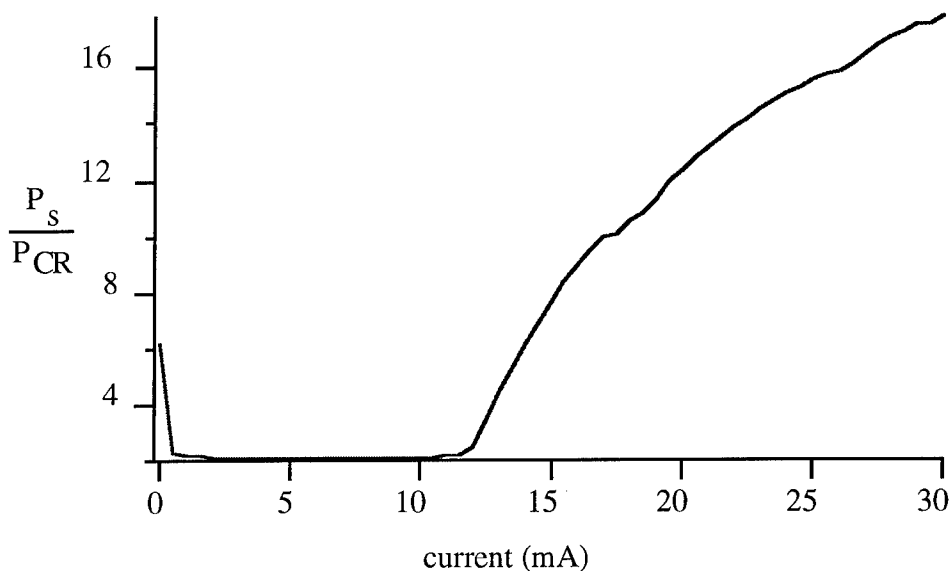


Figure 6: Ratio of output power from standard facet (P_s) to the output power from the CR facet (P_{CR}) as a function of current.

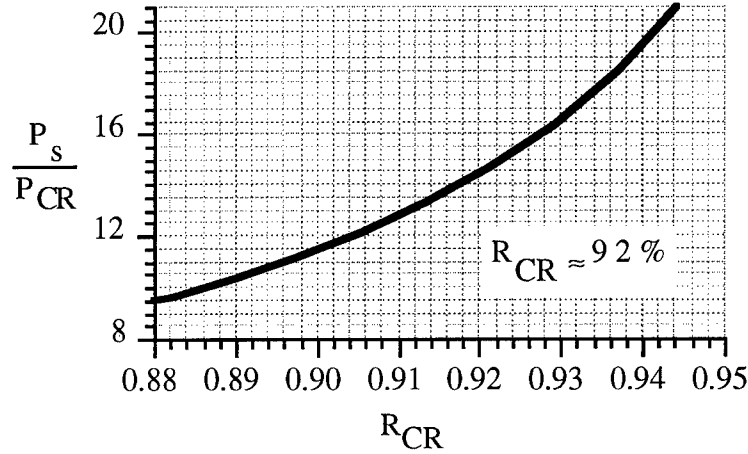


Figure 7: Theoretical output power ratio as a function of the CR mirror reflectivity assuming that the standard facet reflectivity is 32%.

The output power ratio for this device begins to saturate at a ratio of 16, which gives a power reflectivity of approximately 92%. The power reflectivity extracted from Figure 7 indicates that the reflectivity of the CR facet is at least 90%.

Microwave measurements were made with an HP 8510B Vector Network Analyzer controlling an HP 8350B Sweep Oscillator and an HP 8515A S-Parameter Test Set. Full two-port calibrations were performed to move the measurement reference planes to the end of the coaxial microwave probes that were used to supply both a DC bias and RF signal to the laser. An ILX 3620 low noise current source provided the DC bias for the laser via the test set bias tee. The laser output was collimated with a 0.23 pitch (@1300 nm) GRaded INdex (GRIN) rod and then focused into a single-mode fiber using a pigtailed 0.25 pitch GRIN rod/single-mode fiber collimator. The output from the single-mode fiber was sent to a New Focus model 1012 45 GHz detector, and the microwave output of the detector was attached to the test set. Lasers were mounted with indium onto copper carriers which were then attached to a water-cooled copper stage kept at a constant

temperature of 25 °C. In addition, a broad-area Si detector was mounted on the probe station so it could be moved in and out of the beam path. This detector was connected to an HP 4145 parameter analyzer so the CW threshold current could be determined for each laser on the probe station.

Several corner reflector lasers were indium mounted and tested. It was found that the CR lasers with the largest -3dB bandwidths also had cavity lengths of 150 μm . The raw microwave data from a 3 μm \times 150 μm CR laser is shown in Figure 8. The output power for this laser began to saturate near 50 mA and therefore the -3dB bandwidth did not increase much past 20 GHz. The response up to 40 mA is underdamped and does not approach the K-factor limit, i.e. the parasitic free modulation response.

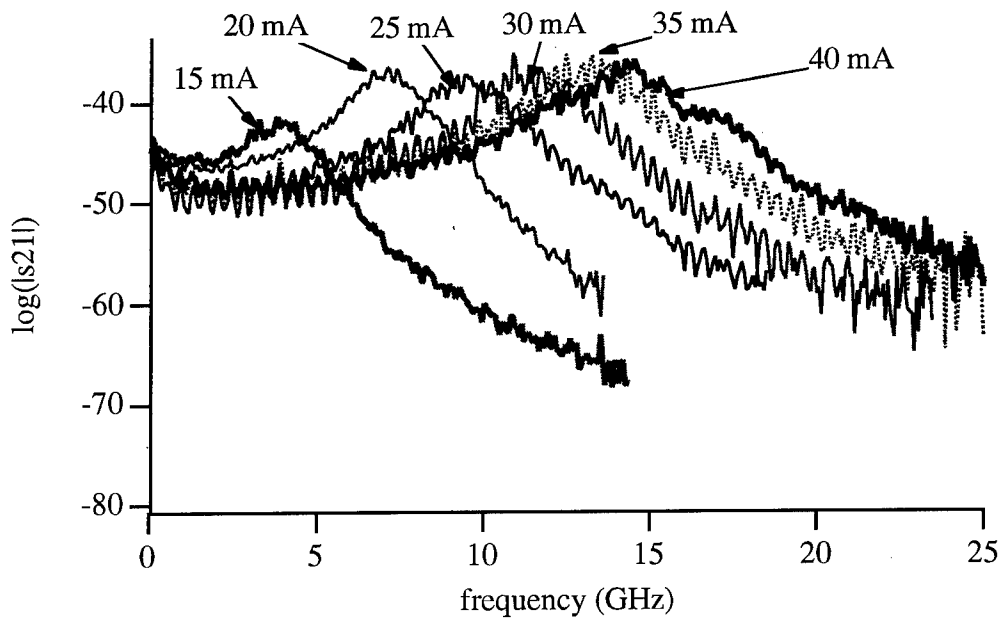


Figure 8: Modulation response of 3 μm \times 150 μm CR laser from 15 mA to 40 mA.

The modulation response shown in Figure 8 was fit to:

$$R(f) = \left(\frac{1}{1 + \left(\frac{f}{f_{\text{par}}} \right)^m} \right) \left(\frac{f_o^4}{(f^2 - f_o^2)^2 + f^2 \left(\frac{\Gamma}{2\pi} \right)^2} \right)$$

where f_o is the resonance frequency, Γ is the damping rate, and f_{par} and m are used as fitting parameters. The only parameters of interest are the resonance frequency (f_o) and the damping rate (Γ), while f_{par} and m were used solely as fitting parameters. This formula provided reasonably good fits with $m < 2$. Since the exact form of the total modulation response (including carrier transport parasitics and electrical parasitics) is rather complex, the above equation was used as an approximation. The problem of extracting resonance and damping information has been discussed by Morton et al.⁹ where they performed a curve fit to a ratio of the measured data at two bias points. They assumed that parasitics were constant as a function of bias. When the parasitics do not vary with bias, the modulation response at one bias can be subtracted from the response at a larger bias to get a response that depends only on the resonance frequency and the damping rate at the two bias points. This method was not chosen since the carrier transport parasitics are not constant with bias.

The damping rate as a function of the square of the resonance frequency for a $3 \mu\text{m} \times 150 \mu\text{m}$ CR laser is shown in Figure 9. The K-factor of 0.06 ns implies a bandwidth of nearly 150 GHz! Even using only the first two data points the K-factor is still 0.11 ns which implies a maximum - 3dB bandwidth of 81 GHz.

The response at 40 mA is still substantially underdamped and is, therefore, not near the intrinsic limit of the material. This saturation of the modulation response below its intrinsic limit has been observed by several authors^{10,11}.

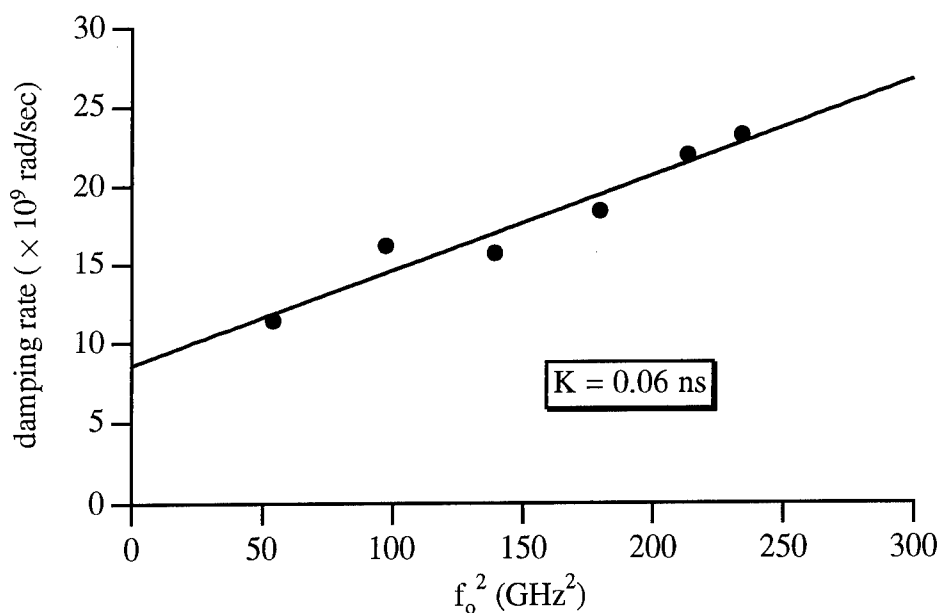


Figure 9: Damping rate vs. square of the resonance frequency for a $3\ \mu\text{m} \times 150\ \mu\text{m}$ CR laser.

To summarize the work that was done on the corner reflector laser project, corner reflector lasers were fabricated with high-reflectivity CR facets with power reflectivities approaching 90% and modulation bandwidths in the low 20 GHz range at a bias of 40 mA. This is the first demonstration of high-speed direct modulation from CR lasers and, to the author's knowledge, is the largest bandwidth for any laser with single-sided output.

DIAMOND HEAT SINKS

The CR and standard lasers that were fabricated had -3dB bandwidths that saturated well below their K-factor limit. Device heating was limiting the performance of these lasers, therefore, improved heat sinks were investigated as a means of controlling the bias current dependent increase of the active region temperature. Diamond heat sinks with (CPW) transmission lines were fabricated. Cleaved facet semiconductor lasers were fabricated and flip-chip bonded to the diamond heat sinks using indium bonding pads. The devices that were flip-chip mounted displayed improved spectral and PI characteristics, indicating that the flip-chip bonding to diamond improved the removal of heat from the active region of the laser. However, the flip-chip bonded lasers did not have larger -3dB bandwidths than unbonded lasers, suggesting that carrier heating was still limiting the high-frequency performance of these devices.

It can be shown that the thermal impedance of a $12\text{ }\mu\text{m} \times 200\text{ }\mu\text{m}$ laser improves by more than a factor of 3 when it is flip-chip mounted to diamond. A breakdown of the thermal impedance analysis is given below. The thermal impedance of the diamond was calculated using a thermal conductivity of 12 W/cm-K for chemical vapor deposited (CVD) diamond. The flip-chip bonded lasers should have a lower active region temperature increase as the bias current is raised due to their smaller thermal impedance. Although the active region temperature of the standard and flip-chip lasers was not measured directly, the differences in the PI and spectral characteristics were consistent with the following thermal impedance analysis:

A. Laser mounted p-side up: $12\text{ }\mu\text{m} \times 200\text{ }\mu\text{m}$ mesa laser

Clad thermal resistance ($1\text{ }\mu\text{m Al}_{0.7}\text{Ga}_{0.3}\text{As}$)	33 °/W
Spreading thermal resistance ($100\text{ }\mu\text{m}$ substrate)	98 °/W
Total thermal resistance	131 °/W

B. Flip-chip mounted laser: $12\text{ }\mu\text{m} \times 200\text{ }\mu\text{m}$ mesa laser

Clad thermal resistance ($1\text{ }\mu\text{m Al}_{0.7}\text{Ga}_{0.3}\text{As}$)	$33\text{ }^{\circ}\text{W}$
Spreading thermal resistance ($300\text{ }\mu\text{m}$ diamond)	$5\text{ }^{\circ}\text{W}$
Total thermal resistance	$38\text{ }^{\circ}\text{W}$

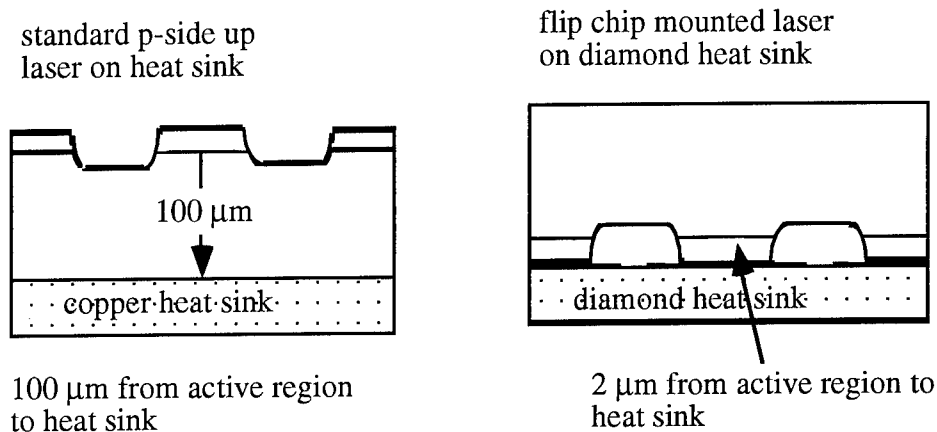


Figure 10: Comparison of the thermal impedance for a $12\text{ }\mu\text{m} \times 200\text{ }\mu\text{m}$ laser bonded p-side up on a standard heat sink and flip-chip bonded to a diamond heat sink.

Diamond heat sinks were fabricated in collaboration with GE Superabrasives. Processing was done on $1\text{ cm} \times 1\text{ cm}$ CVD diamond squares. The overall fabrication sequence is illustrated in Figure 11 on the following page.

The fabrication sequence involved only three major steps: (a) CPW fabrication, (b) indium solder pad deposition, (c) laser scribing of individual heat sinks and flip-chip bonding lasers to heat sinks. Fabrication of the transmission lines was done at Cornell and GE. Ti/W/Au coplanar waveguide lines were fabricated with a liftoff process, where the lithography was done at Cornell

and the metal sputter deposition of 5000 Å of Ti/W/Au was done at GE. After the CPW lines were fabricated, their scattering parameters were measured with a vector network analyzer, shown in Figure 12. The match over the entire frequency range was relatively good.

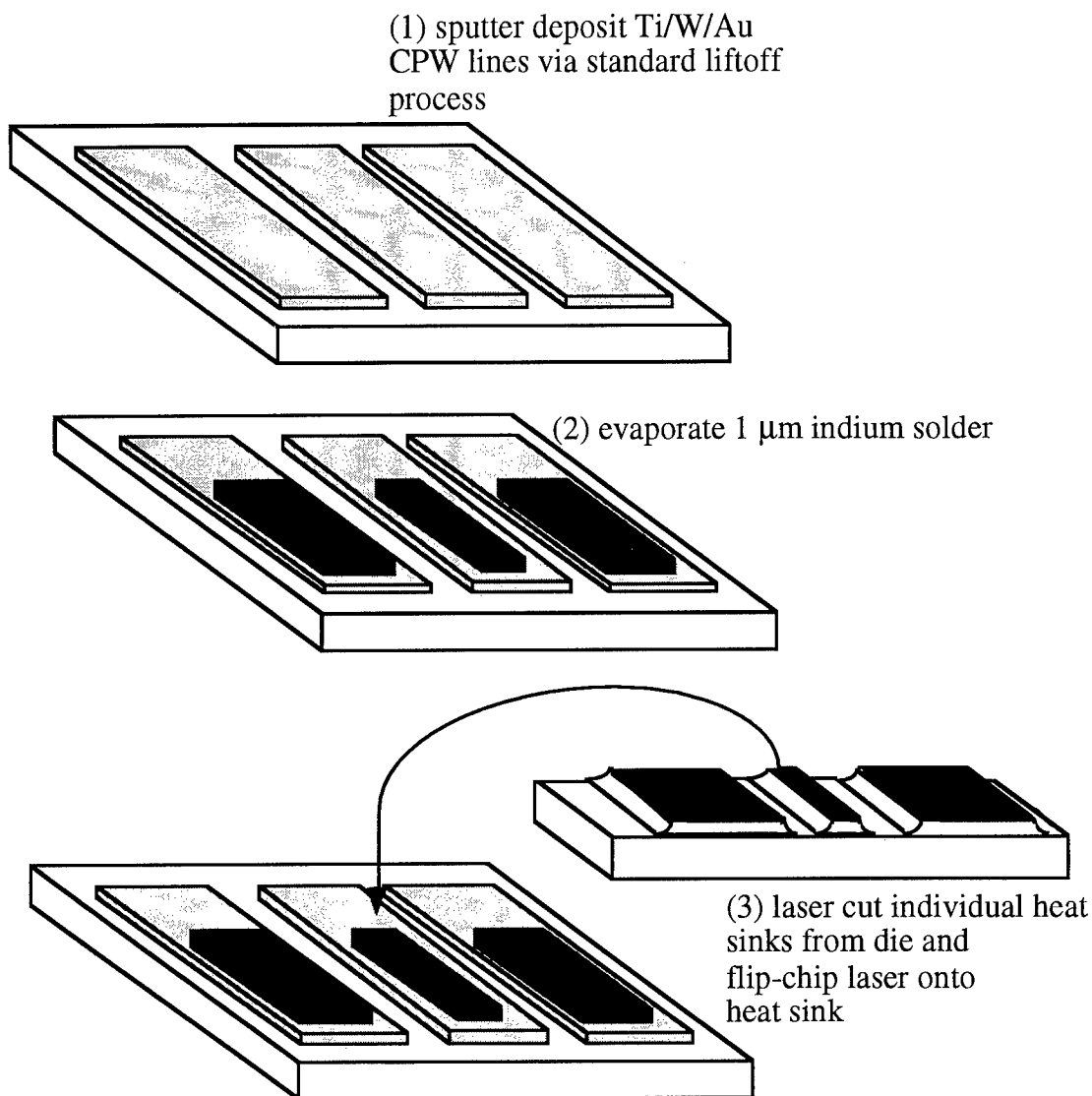


Figure 11: Fabrication sequence for lasers flip-chip mounted on diamond heat sinks.

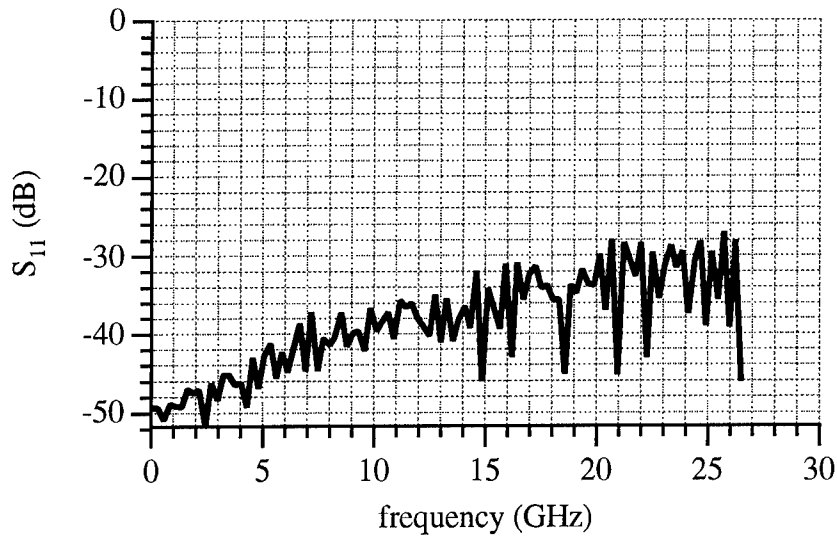


Figure 12: Plot of measured S_{11} of CPW lines on diamond.

Indium was chosen as the solder material. It has a low melting temperature (156 °C) and can be easily evaporated, thus making the fabrication of indium bonding pads through a standard lift-off process possible. In addition, the abundant supply of indium in our MBE laboratory made it the logical choice for a solder material. All indium depositions were performed on a refurbished evaporator that was used solely for indium. Test evaporations were done on blank silicon wafers to determine the optimum conditions for indium deposition. Smooth indium films on silicon were achieved for evaporation rates between 70 Å/min. -100 Å/min. After completing the lithography for the heat sink contact pads, approximately 1 µm of indium was evaporated. The indium deposition on the gold was substantially rougher than the test evaporations on silicon, but still suitable for the flip-chip bonding process. The final step in the fabrication sequence was to laser cut the individual heat sinks from the 1 cm × 1 cm die. Before laser cutting the diamond, photoresist was spun over the diamond chip and a quick lithography run was performed to reveal

the 'streets' in the resist where the laser would cut out individual heat sinks. The resist was used to protect the CPW lines from the formation of a conductive graphite film that accompanies laser ablation of CVD diamond¹². This graphite film has the potential to short the ground and signal pads together, and in fact, did so on several heat sinks. After protecting the heat sinks with the resist layer they were sent to GE for laser cutting. Upon their return to Cornell, individual heat sinks were separated from the backing tape that held them in place with an acetone soak and then rinsed in isopropyl alcohol. They were then cleaned in an acetone ultrasonic bath for several hours to remove any residual graphite from the surface of the diamond.

Flip-chip bonding was performed with a commercial flip-chip bonder¹³. This bonder was obtained by Rome Laboratory for the purpose of flip-chip bonding VCSELs. Since most of the initial characterization work for flip-chip bonding had been completed for the VCSEL project, only a few modifications were made to flip-chip bond edge emitting lasers.

The bonded laser/heat sink is shown in Figure 13 and Figure 14 on the next page. Even with the large amount of automation, the yield in the bonding process was typically 50% or less. Some of this was due to the small sizes of the pieces that were being handled. Nonetheless, the bonding that was achieved produced several working, flip-chip bonded lasers that did show improvements in their DC performance.

The effectiveness of the flip-chip bonding was characterized by pulsed and CW measurement of the output power as a function of input current. The PI test setup used a ILX LDP-3811 pulsed current source, a high-speed germanium photodetector with a Thor Labs bias control, and an EG&G boxcar averager. The germanium detector was calibrated at the factory and the calibration data was used in the LabView[®] program that controlled the operation of the PI test setup. Spectral

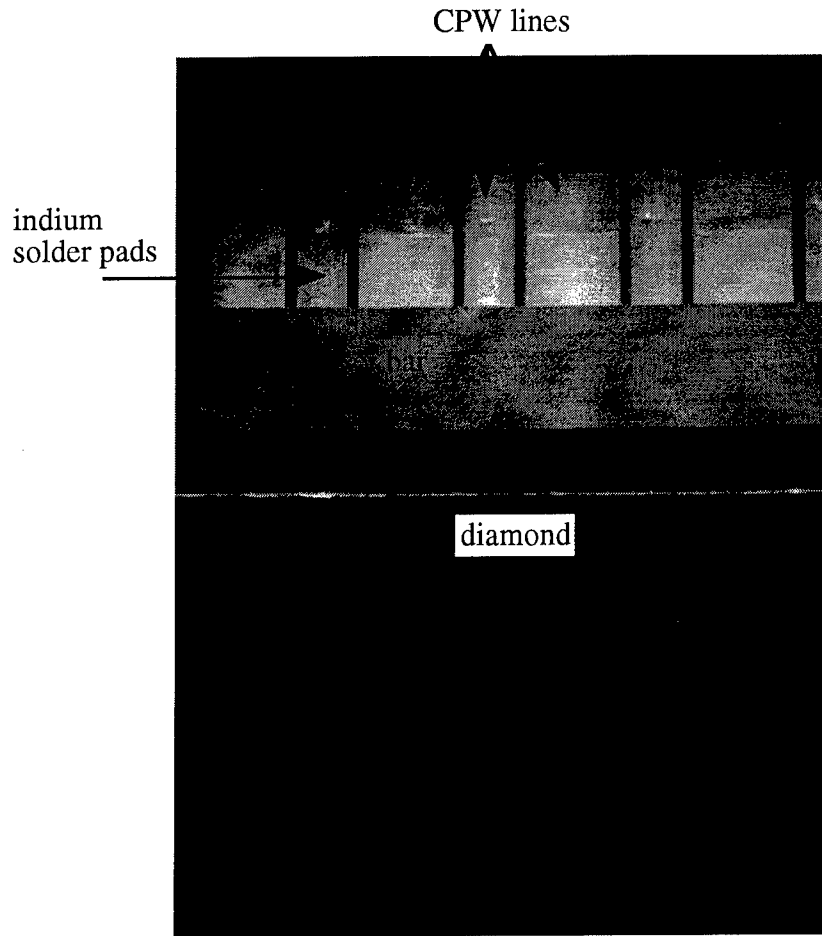


Figure 13: SEM of a 200 μm long laser flip-chip bonded to a diamond heat sink.

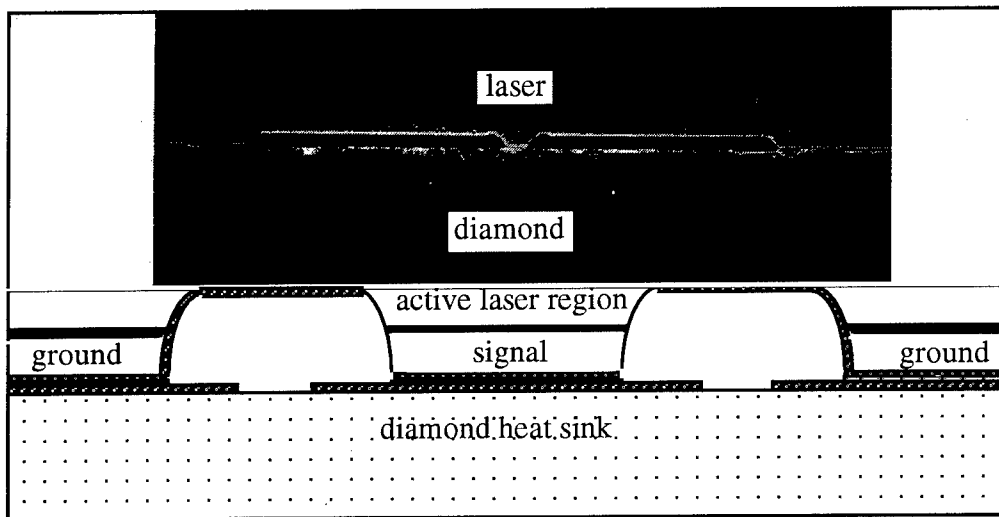


Figure 14: SEM and schematic of laser flip-chip bonded to diamond heat sink.

data was collected with an HP 70951A Optical Spectrum Analyzer (OSA). Optical input to the OSA was through a single mode fiber, so the output of the laser under test was collimated with a 0.23 pitch (@1300 nm) GRIN rod and focused into the single mode fiber with a Newport single mode fiber coupler. Another LabView[®] program was written to track the wavelength of a single Fabry-Perot mode as a function of current using the OSA and the current source. The overall test setup is shown in Figure 15.

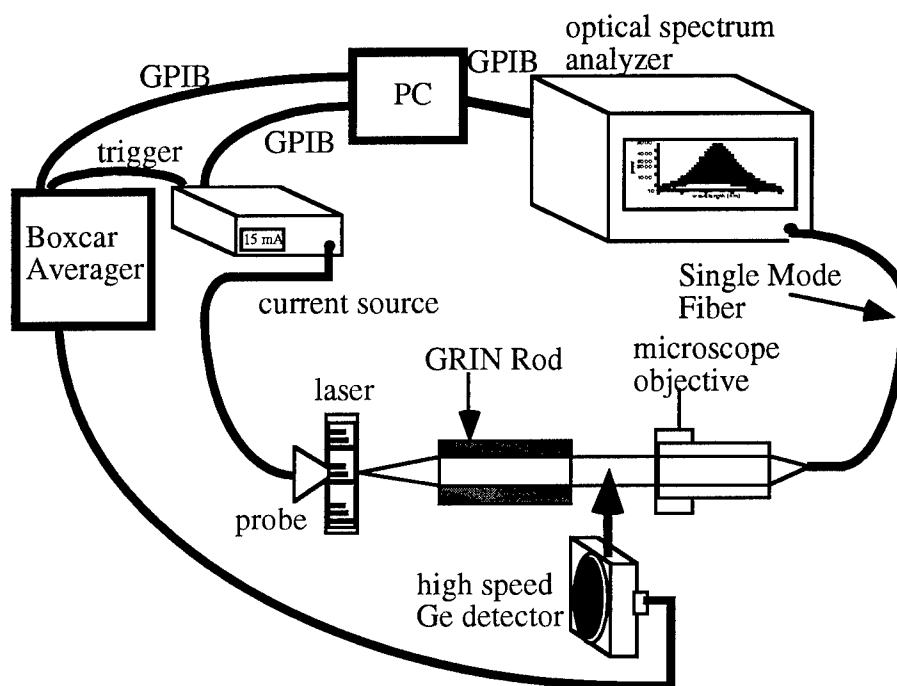


Figure 15: Test setup for DC and spectral characterization of lasers.

Several cleaved facet lasers were flip-chip bonded to the diamond heat sinks. Eight bars (8 lasers on each bar) were bonded to heat sinks. The number of working devices after bonding ranged from 2 to 5 lasers per bar. Usually, one side of the laser/heat sink was found to be an open circuit;

a result of the laser and the heat sink not being exactly parallel to each other. In addition, some of the working devices were degraded after the bonding, with measured threshold currents that were higher than the threshold currents of the laser bar alone. Out of a total number of 64 lasers that were bonded, 35 survived the bonding process. For devices that were well bonded, the improvement in the DC performance was significant. This is especially true for the working 200 μm lasers. Figures 16 and 17 show the PI curves for an unbonded and flip-chip bonded 12 $\mu\text{m} \times 200 \mu\text{m}$ laser.

The total output power that was measured from the flip-chip bonded laser is somewhat lower than the total power collected from the unbonded device due to the increased facet-to-detector distance in the flip-chip bonded laser. The unbonded laser shows a significant roll off of the optical power as the duty cycle is increased, indicating that a substantial amount of bias dependent heating is taking place. On the other hand, the quasi-CW and the pulsed PI measurements are almost identical in the flip-chip bonded laser. There were no cases of unbonded lasers that did not display the rollover in the CW PI characteristics from this wafer, while about 1/3 of the tested, working flip-chip bonded lasers showed significant improvement in the CW PI measurements. Although the yield of the flip-chip process was not large, the improvement in the PI characteristics of successfully bonded lasers was significant.

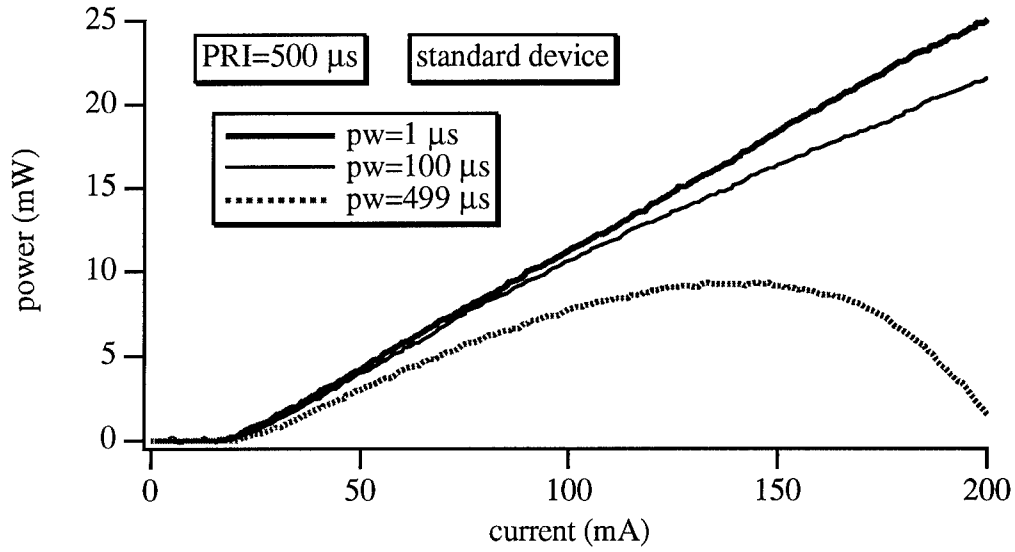


Figure 16: Output power for an unbonded $12\ \mu\text{m} \times 200\ \mu\text{m}$ laser from wafer 4002. The pulse repetition interval is $500\ \mu\text{s}$; therefore the duty cycle of the three measurements are 0.2%, 20%, and 99.8%.

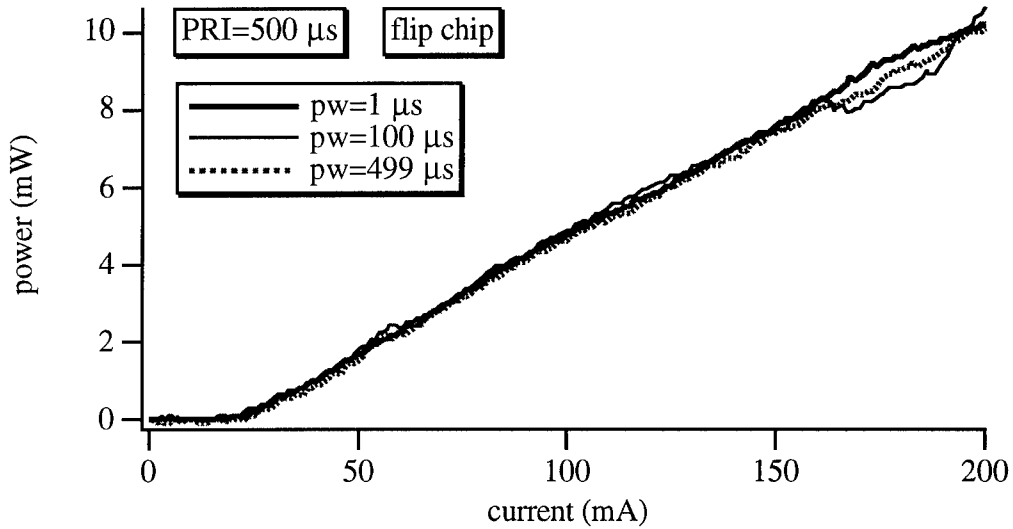


Figure 17: Output power for a flip-chip bonded $12\ \mu\text{m} \times 200\ \mu\text{m}$ laser from wafer 4002 under the same test conditions as the previous figure.

Further evidence of the reduced thermal impedance of the flip-chip bonded lasers was obtained by an examination of the spectral characteristics of the lasers. Information on the shift in the wavelength of an individual Fabry-Perot (FP) mode as a function of bias gives information on the bias dependent temperature increase in the laser. To determine the effect of increasing the current on the FP wavelength, the factors that affect the wavelength must be identified. Below threshold, both the carrier concentration and the temperature are increasing with bias. Since the refractive index (μ) is a function of the carrier density and the temperature, the wavelength of an individual FP mode is also a function of carrier density and temperature. Above threshold, the carrier density is clamped (ideally), and therefore, the FP wavelength is only a function of temperature. The refractive index varies as $\mu = b_n$, where μ , b , and n are the refractive index, a material constant, and the carrier concentration¹⁴, and the FP wavelength is given as $\lambda_m = 2L\mu/m$ where L is the cavity length and m is an integer. Thus, below threshold, the variation in the FP wavelength due to the change in carrier density and temperature is:

$$\frac{d\lambda_m}{dI} = \frac{2L}{m} \left(\frac{\partial \mu}{\partial n} \frac{\partial n}{\partial I} + \frac{\partial \mu}{\partial T} \frac{\partial T}{\partial I} \right).$$

The only term that is negative is $\partial \mu / \partial n$. Therefore, the change in wavelength has two components. The decrease in the refractive index with increasing current (carrier density) causes the wavelength to decrease, while the increase in refractive index with increasing temperature (carrier density) causes the wavelength to increase with bias. The relative magnitude of each process will determine whether or not the wavelength increases or decreases as a function of bias.

Above threshold, the carrier density is approximately clamped, and the change in the FP wavelength is due only to the change in temperature as:

$$\frac{d\lambda_m}{dI} = \frac{2L}{m} \left(\frac{\partial \mu}{\partial T} \frac{\partial T}{\partial I} \right).$$

Therefore, the FP wavelength increases with current above threshold. The wavelength of a FP mode as a function of bias is shown in Figure 18 and Figure 19 for the same bonded and unbonded lasers whose PI curves were shown in Figure 16 and Figure 17.

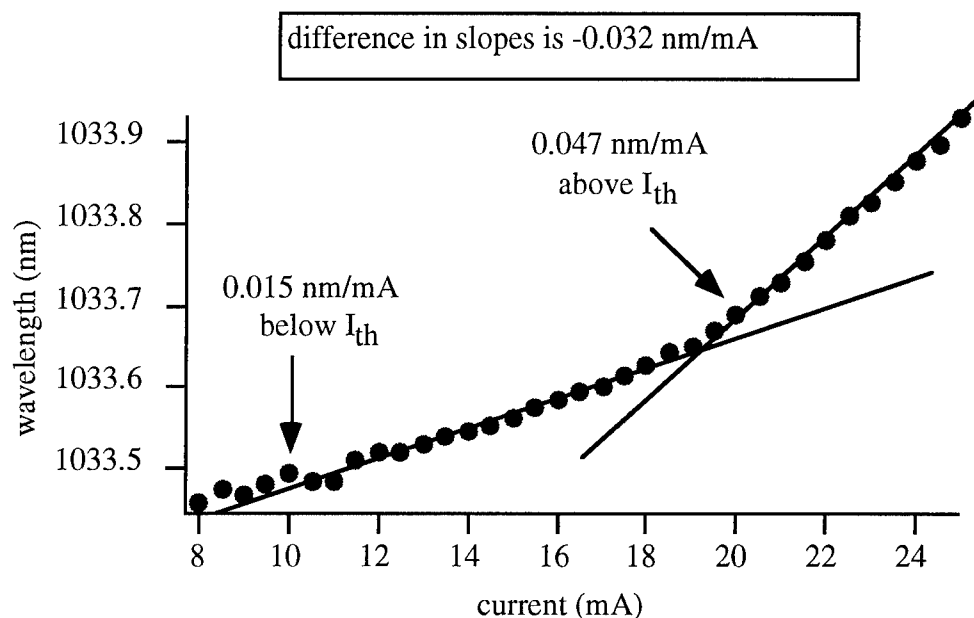


Figure 18: Wavelength of a FP mode vs. current density for a 12 $\mu\text{m} \times 200 \mu\text{m}$ unbonded laser.

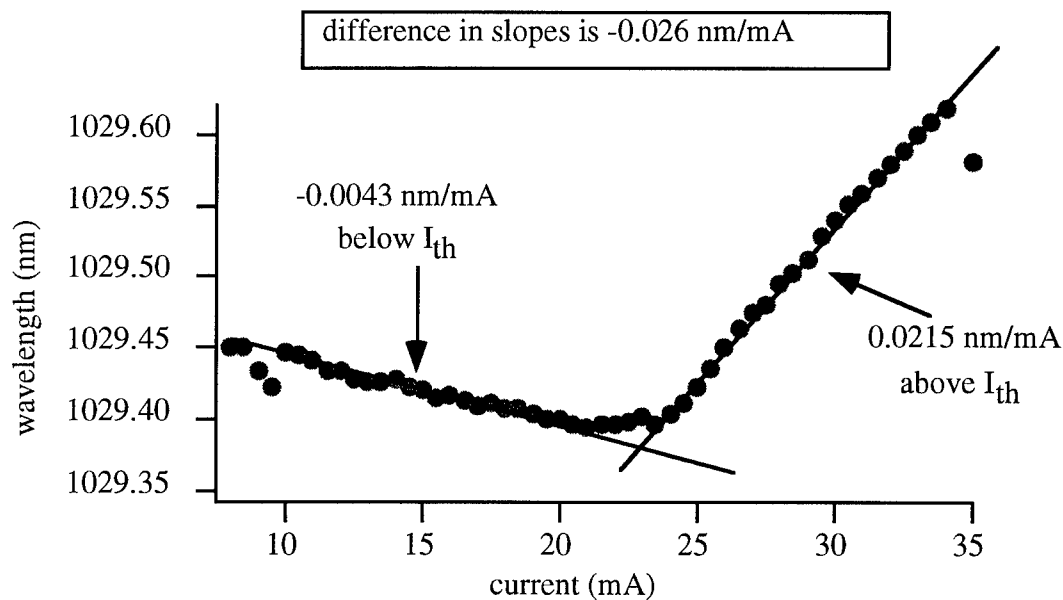


Figure 19: Wavelength of a FP mode vs. current density for a 12 $\mu\text{m} \times 200 \mu\text{m}$ unbonded laser.

The effective bias dependent temperature increase for the flip-chip bonded laser is reduced, as seen by the lower value of $d\lambda/dI$ after threshold. In fact, $d\lambda/dI$ of the flip-chip bonded laser is nearly one-half the post-threshold value of $d\lambda/dI$ for the unbonded laser. This indicates that the flip-chip bonded laser does indeed have a smaller thermal impedance than the unbonded laser.

The different in slope of $\lambda(I)$ before and after threshold are calculated for the bonded and unbonded laser. The difference in the slope before and after threshold is proportional to the change in the refractive index as a function of current (carrier density). In the flip-chip bonded laser, this value is equal to -0.032 nm/mA, while in the bonded laser it is equal to -0.024 nm/mA. This difference in the slope before and after threshold should give the magnitude of the change in the refractive index as a function of current injection and should therefore be negative. The fact that there appears to be a difference in the change in the refractive index as a function of carrier density for the two lasers is more likely due to experimental error rather than some physical difference. Measurements of the change in wavelength versus current using a pulsed current source to eliminate lattice heating gave a value of $d\lambda/dI = -0.031$ nm/mA for this laser structure, which is nearly identical to the value from the unbonded laser. These spectral measurements are consistent with the PI curves shown in Figure 16 and Figure 17, and give further evidence that the lattice heating in the laser has been reduced in the laser that was flip-chip bonded to a diamond heat sink.

Microwave measurements were made in the manner described previously to determine the high-frequency characteristics of lasers that were flip-chip bonded to diamond heat sinks.

Measurements of lasers that were flip-chip bonded to diamond did not see any substantial improvement either in the resonance frequency or in the overall achievable bandwidth. In fact, the maximum bandwidth that was achieved on any of the flip-chip bonded or unbonded lasers was only 15 GHz. This modest bandwidth is, in part, due to the material design and the fabricated

laser structure that was chosen for the bonding experiment. They were all cleaved facet lasers with cavity lengths ranging from 200 μm to 400 μm . Although the use of relatively long cleaved facet lasers greatly simplified the processing, they were far from the optimum cavity length for microwave performance. The best bandwidth achieved from this wafer was 23 GHz from a 3 μm \times 100 μm ridge waveguide laser. Several changes in the dry-etch laser process sequence would need to be made to make them compatible with flip-chip bonding. The mirrors would still be dry-etched, but the fabrication of the contact mesas would need to be done with either a wet etch or an angled dry etch. Simply performing an additional step-metallization would not provide a sufficiently planar top contact area. Although the additional processing steps would complicate the overall fabrication sequence, it should be possible to fabricate short cavity lasers and then flip-chip bond these laser to diamond heat sinks. Any improvement in the DC characteristics of short cavity lasers that were flip-chip bonded to diamond should directly translate into improved high-frequency characteristics.

The flip-chip bonding project was meant to complement the work that was going on in other areas of material and design optimization in GaAs and InP based lasers. By extracting the maximum performance from any particular design the overall bandwidth can be increased. This first set of flip-chip bonding tests were promising, with the flip-chip bonded devices showing a substantial improvement in their DC characteristics. Although the long cavity lasers that were bonded did not show an improvement in their modulation bandwidth the work here was nonetheless an important first step in understanding the thermal limitations on directly modulated semiconductor lasers.

CARRIER HEATING AND CARRIER TRANSPORT

In the last decade, intensive work has been done to investigate the small signal modulation response of semiconductor quantum well (QW) lasers, and tremendous efforts have been taken to optimize their high-speed performance for achieving a maximum modulation bandwidth. Recently, QW lasers with a record modulation bandwidth of over 40 GHz have been successfully demonstrated. It is not surprising to find that a gap still exists between experimental reality and the optimistic theoretical estimations predicting an achievable 60~90 GHz modulation bandwidth. Therefore, it is highly desirable to theoretically study what is the major limitations on the modulation bandwidth of QW lasers. So far, three major physical mechanisms have been attributed for the limitation on the modulation bandwidth of QW lasers: spectral hole burning, carrier heating, and carrier transport, and the time constants associated with these physical processes are the carrier dephasing time, carrier energy relaxation time, and carrier diffusion-capture-escape times respectively.

To investigate the effects of spectral hole burning, carrier heating, and carrier transport on the modulation bandwidth of QW lasers, we have developed a comprehensive model that includes the following features:

- (1) To exactly describe the interaction between carriers, photons, and phonons in the QW lasers, we derived a set of rate equations in our theoretical model from the carrier Boltzmann equation, Maxwell's equations, and phonon Boltzmann equation and thus eliminate any unnecessary error associated with the phenomenological models (see Figure 20).

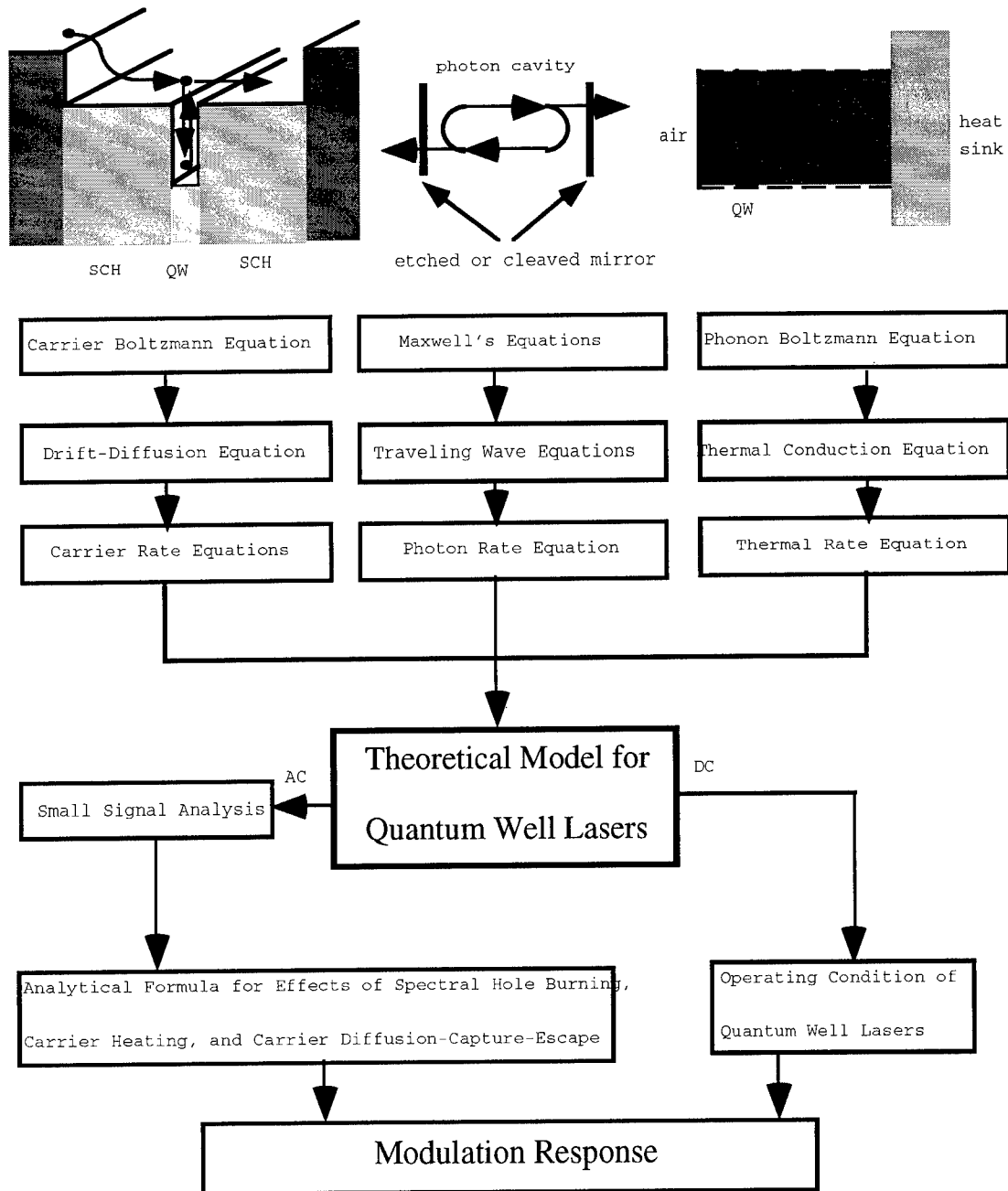
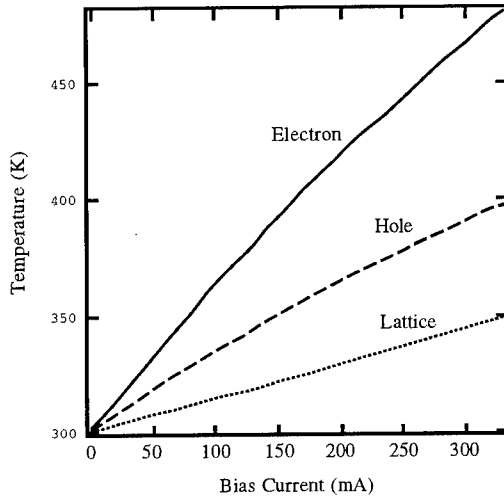
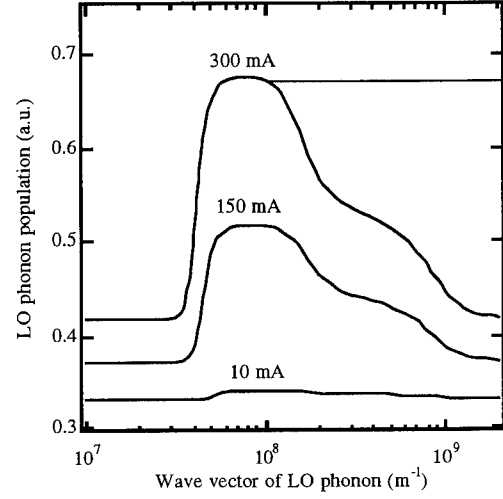


Figure 20: Schematic diagram of the theoretical framework used to describe quantum well lasers.

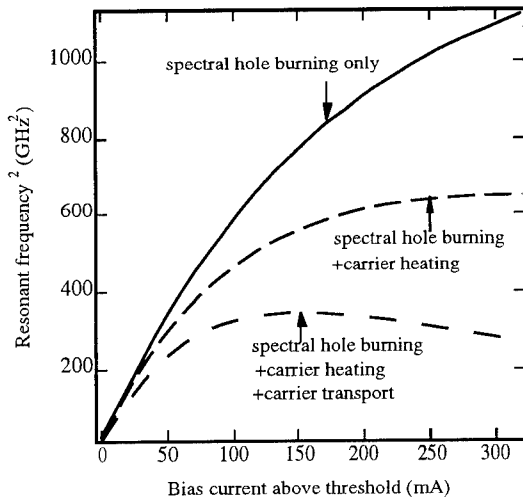
- (2) To make our theoretical model more realistic and accurate, we calculated the carrier dephasing time, carrier energy relaxation time, and carrier quantum capture and escape times from first principles instead of assigning arbitrary time constants as the conventional approaches.
- (3) Since these three physical processes mutually influence each other, we simultaneously consider their effects on the small-signal modulation response of QW lasers, instead of separately focusing on one or two of these physical processes as does the conventional approach.
- (4) From our theoretical model, we numerically determine the temperatures of electrons, holes, and lattice in the operating condition of QW lasers. We also simulate the population distribution of longitudinal optical (LO) phonons by incorporating the hot phonon effect in QW lasers (see Figure 21).
- (5) To investigate the effects of these physical processes on the small-signal modulation response of the QW lasers, we perform an elaborate small signal analysis on our rate equations and obtain an exact analytical solution for the modulation response of QW lasers. From our exact small signal analysis, the nonlinear gain coefficients associated with the effects of spectral hole burning, carrier heating, and carrier transport are thus unambiguously defined. Their relations with the modulation bandwidth of QW lasers are rigorously derived.



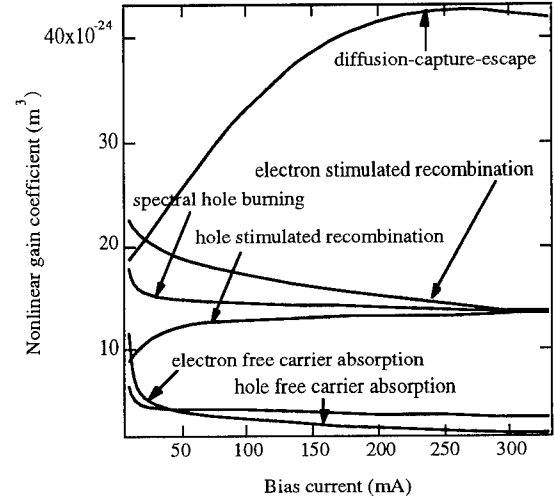
(a)



(b)



(c)



(d)

Figure 21: (a) Electron temperature, hole temperature, and lattice temperature as a function of the bias current in a $50\text{\AA} \times 3\mu\text{m} \times 500\mu\text{m}$ $\text{Al}_{0.3}\text{Ga}_{0.7}\text{As}/\text{GaAs}$ SCH single QW laser. The width of the SCH is 1000\AA . The length between the QW and the heat sink is $100\mu\text{m}$. (b) Population distribution of LO phonons as a function of LO phonon wave vector at different bias currents. (c) Square of the resonant frequency vs. the bias current above threshold. (d) Nonlinear gain coefficients due to the effects of carrier diffusion-capture-escape, spectral hole burning, stimulated recombination heating, and free carrier absorption heating.

Several interesting results are obtained from our theoretical model:

- (1) Carrier capture and escape times in an AC condition are significantly different from a DC condition. Our results indicate that the conventional theoretical models that do not distinguish the differences between the DC and AC capture and escape times may underestimate the influence of carrier transport processes on the modulation bandwidth of QW lasers.
- (2) Our first-principle calculations show that the DC escape time predicted by the classical thermionic emission theory is no longer valid if the width or depth of the QW is small. Therefore, in that case, the first principle calculation is indispensable for estimating the carrier escape time in QW lasers.
- (3) Contrary to conventional belief, our small-signal analysis shows that the nonlinear gain coefficient due to free carrier absorption affects only the damping rate of the modulation response of semiconductor lasers but not the resonant frequency.
- (4) Since it takes about 3 ps for LO phonons to decay into acoustic phonons at room temperature, this will cause the hot phonon effects on the carrier energy relaxation processes. Our theoretical calculations indicate that neglecting these hot phonon effects will underestimate the carrier energy relaxation time by almost an order of magnitude and thus severely underestimate the effects of carrier heating on QW lasers. Therefore, it is very crucial to take these hot phonon effects into account when modeling the carrier heating of QW lasers.
- (5) As the carrier temperature increases due to the effects of carrier and lattice heating, more carriers will escape from the QW and fewer carriers will be captured into the QW. At high bias current levels, this mechanism will severely degrade the resonant frequency, significantly increase the nonlinear gain coefficient due to carrier transport (see Figure 21), and thus, ultimately limit the modulation bandwidth of QW lasers.

From our theoretical study, we identified the enhancement of carrier escape (overflow) processes due to the effects of carrier and lattice heating as the major physical mechanism that limits the modulation bandwidth of QW lasers; therefore, it is very crucial to reduce the magnitude of carrier or lattice heating if we want to improve the modulation bandwidth of QW lasers. To reduce the lattice heating, we can use the flip-chip scheme on the laser device. This will shorten the path of thermal conduction from the QW to the heat sink by more than an order of magnitude. Our theoretical results also indicate that using p-doping in the active region of QW lasers will provide an additional channel for electrons to relax their energy to holes by electron-hole scattering and may reduce the electron temperature.

We have focused most of our theoretical effort in studying the small-signal amplitude modulation (AM) response of QW lasers (i.e., in the frequency domain). It will be straightforward to use our theoretical model to analyze other modulation schemes, such as FM, PM, ASK, FSK, and PSK and their large-signal behavior. Issues like chirp and intermodulation distortion can thus be characterized in detail. Moreover, our theoretical model can also be implemented to investigate the effects of spectral hole burning, carrier heating, and carrier transport in the gain switch or mode locked of the short-pulse QW lasers (i.e., in the time domain). Incorporating the noise model into our theoretical frame, we hope that our comprehensive theoretical model can predict the overall dynamic behavior of semiconductor QW lasers.

(111)-ORIENTED LASERS

Although all conventional means for attaining 1.3 μm wavelengths employ InP substrates, we sought for a method to reach this longer wavelength in a GaAs-based device. The reasons for investigating this possibility include:

- (1) InGaAs/GaAs based devices have demonstrated much more uniform performance with temperature fluctuations than InP-based devices which would generally require integrated temperature control in any device package to insure stability¹⁵.
- (2) The InGaAs/GaAs material system has demonstrated world record modulation bandwidths in excess of 40 GHz while InP-based devices have been limited to the low to mid 20 GHz due to problems with optical and electrical confinement [ref. to Weisser].
- (3) Currently, low dislocation density GaAs substrates are readily available and inexpensive while high quality InP production technology lags behind that of GaAs.
- (4) The GaAs material system is well characterized, and device processing technologies are much more mature than in the InP-based system.

To achieve this goal of extending the wavelengths available to the InGaAs/GaAs material system, we investigated several possibilities. Some researchers have grown metamorphic layers¹⁶ to increase the lattice constant and decrease the bandgap, while others have attempted to use a bilayer quantum well using Sb to achieve longer wavelengths¹⁷. While both these methods have been successful in reaching 1.3 μm , we concluded that neither would be conducive to high speed modulation. The first would introduce too many dislocations leading to device heating and poor performance while the second spatially separates electrons and holes reducing the overlap of the envelope functions. We did, however, develop a means for extending the wavelengths of this

material system that we believe holds promise for achieving large directly modulated bandwidths that would surpass those currently achievable on InP substrates. Our calculations have shown that by incorporating an ordered $(\text{InAs})_1(\text{GaAs})_1$ monolayer superlattice in the active region of a laser diode based on GaAs(111), wavelengths well beyond $1.3\text{ }\mu\text{m}$ are theoretically possible.

The (111) orientation has two very important advantages over the standard (001) direction that we take advantage of to narrow the bandgap. First, the Matthews-Blakeslee critical thickness for pseudomorphic layers in the (111) direction is approximately twice that of (001) layers. This larger critical thickness allows for quantum well designs that incorporate higher Indium contents at reasonable well widths. Although we have found that this advantage alone does not accomplish the task of reaching $1.3\text{ }\mu\text{m}$, this does allow for quantum wells with 50% Indium up to the critical thickness of $90\text{ }\text{\AA}$, for example. This particular composition of $\text{In}_{0.5}\text{Ga}_{0.5}\text{As}$ is important for the second part of our proposed structure, an ordered quantum well. Unlike the case of the random alloy, the occupation of the lattice sites in an ordered ternary are known with certainty. This is shown schematically in Figure 22.

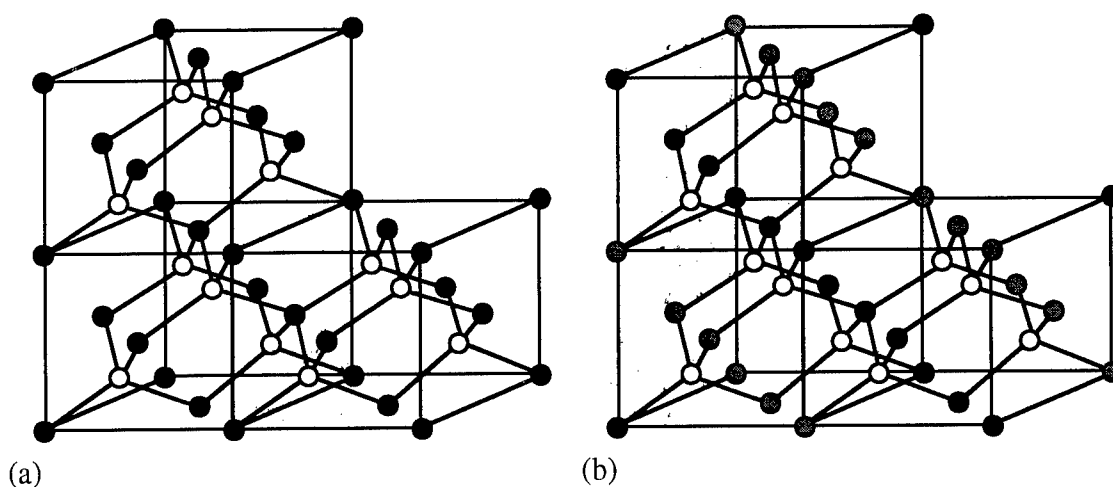


Figure 22: Zincblende structure for a mixed group III ternary for the case of (a) an ideal alloy and (b) for a CuPt ordered structure. The white atoms represent the common group V element while the black and gray in (b) represent the two group III elements. The dark gray element in (a) represents the randomly occupied group III lattice sites.

In the ideal random alloy, the lattice sites are randomly occupied with probabilities given by the material composition. In the case of CuPt ordering that we have considered, the two group III elements form alternating planes in the (111) direction. The band structure for this monolayer superlattice of $(\text{InAs})_1(\text{GaAs})_1$ is very different from the compositionally equivalent $\text{In}_{0.5}\text{Ga}_{0.5}\text{As}$ alloy. First of all, with the lattice positions no longer random, the reduced symmetry of the CuPt structure introduces a crystal field splitting at the top of the valence band similar to that caused by strain. Secondly, ordering along the (111) direction leads to a splitting between the original Γ states and the original L states that are now folded onto the zone center due to the superlattice perturbation. This bandgap reduction has been predicted to be on the order of 350 meV in a perfectly ordered crystal. Although similar effects occur for ordering along the (001) direction, the calculated narrowing has been found to be approximately 60 meV.

We have calculated the zone center transition wavelengths for a device based on GaAs(111) incorporating a strained $(\text{InAs})_1(\text{GaAs})_1$ quantum well with GaAs barriers. Although we found that wavelengths up to and beyond 1.7 μm are theoretically possible for a perfectly ordered well at the Matthews-Blakeslee critical thickness, we do not believe that these results are technologically realizable. However, we do believe that this system is promising for producing 1.3 μm emission simply by tailoring the well width and degree of partial ordering in the well. In Figure 23 we show constant wavelength curves for various combinations of well width and ordering. The ordering parameter, η , in this figure measures the degree of ordering where the random alloy case is given by $\eta=0$, and the perfectly ordered case corresponds to $\eta=1$. If growth conditions can be found to produce even a moderate degree of ordering like 0.6, then a well-width of approximately 70 Å will produce 1.3 μm emission. Already, ordering as high as $\eta=0.66$ has been reported in the GaInP/GaAs material system¹⁸. Therefore, we believe that such devices are not only feasible, but well within the range of current technology.

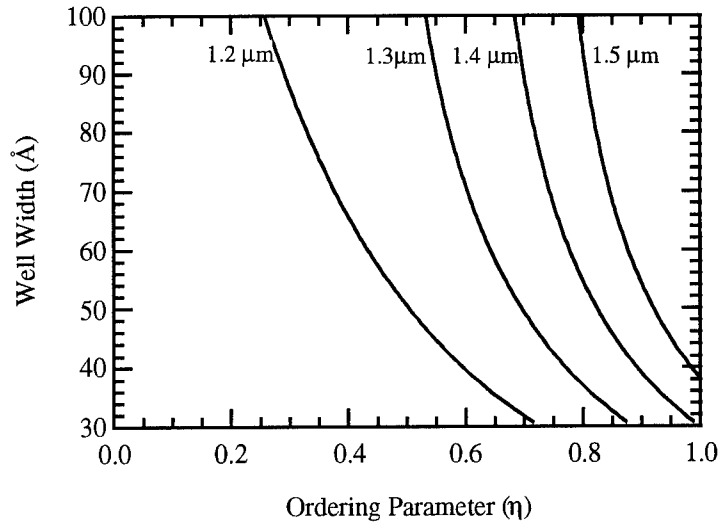


Figure 23: Constant wavelength curves for an $\text{In}_{0.5}\text{Ga}_{0.5}\text{As}$ quantum well with GaAs barriers oriented in the (111) direction. The curves are, from left to right, the necessary combinations of partial long-range ordering and well width for 1.2 μm , 1.3 μm , 1.4 μm , and 1.5 μm transition wavelengths at the zone center. The Matthews-Blakeslee critical thickness for this well is approximately 90 Å.

Several experimental and theoretical results indicate the potential for (111)-oriented lasers to outperform current InP-based laser diodes at 1.3 μm :

- (1) (111) GaAs/AlGaAs SCH lasers had lower threshold current densities than simultaneously grown (001) devices. The higher efficiency was attributed to a larger optical transition matrix element and a shorter carrier capture time¹⁹.
- (2) Theoretical investigations have shown that (111)-based devices should have smaller linewidth enhancement factors than their (001) counterparts improving differential gain²⁰.
- (3) Larger conduction band offsets in GaAs-based diodes should produce less heterobarrier carrier leakage than in the InP material system improving the temperature stability of

these devices. Additionally, the deeper quantum wells afforded by the InGaAs/GaAs diodes should increase the carrier escape time and thereby improve the external differential gain.

- (4) The larger index of refraction step between guide and cladding materials for GaAs-based lasers will improve the optical confinement of the lasing mode and thereby produce higher modal gains than InP laser diodes.

Because of these improvements, we believe that these devices will produce 1.3 μm emission with higher directly modulated bandwidths than current state-of-the-art InP-based laser diodes.

SUMMARY AND FUTURE WORK

Although the overall objective was not achieved, i.e. 44 GHz lasers at 1.3 μm , this project nonetheless did produce several important results:

- (1) Several very detailed, theoretical models of the direct modulation of semiconductor lasers were produced that, for the first time, simultaneously included the effects of carrier diffusion, capture, escape, and heating.
- (2) An analytical density of states formula was described to assist in the modeling of semiconductor lasers, and has in fact been used by our colleges at the IAF to model their results²¹.
- (3) High-speed directly modulated corner reflector lasers with single-sided output were designed, fabricated, and tested. These lasers have the largest direct modulation bandwidth (20 GHz) of any single-sided output laser yet produced, achieving 20 GHz bandwidths within the next year.
- (4) Diamond heat sinks were fabricated with 50 Ω CPW transmission lines. Cleaved facet lasers flip-chip bonded to these heat sinks were tested. We determined that the DC and spectral characteristics of these lasers were greatly improved over unbonded devices.

The theoretical work that was done showed that there are no inherent physical limitations to the direct modulation bandwidth below 60 GHz. The present state-of-the-art bandwidths (near 40 GHz) are primarily limited by lattice and carrier heating. Our initial experimental results show that

carrier heating may indeed be the ultimate limitation of the modulation bandwidth, and therefore novel methods for reducing the carrier heating may be necessary.

Further optimization of directly modulated semiconductor lasers should proceed in two major areas:

- (1) The heat sink technology must still be improved further. Improved heat sinks will benefit all classes of lasers, from VCSELs to DFB lasers intended for cable TV distribution. This type of work has shown a great deal of promise during the initial testing that was done here for both VCSELs and edge emitting lasers. However, more work must be done to increase the yield of the heat sinking process.
- (2) More work on novel 1.3 μm lasers is needed. This should include, and perhaps focus on, stress-compensated lasers and (111)-oriented lasers. This type of growth optimization will most likely be expensive in terms of money and manpower, but shows tremendous promise in terms of improving all aspects of long wavelength semiconductor lasers. This is especially true in the temperature sensitivity of 1.3 μm and 1.55 μm semiconductor lasers, which can be drastically improved with stress-compensated structures. Research into optimized material designs will yield improvements in almost every area of long-wavelength semiconductor laser operation. In addition, the work in this material system will benefit not only edge emitting lasers, but will also improve VCSEL lasers for high temperature operation.

REFERENCES

- ¹ E.C. Larkins, W. Benz, I. Esquivias, W. Rothmund, M. Baeumler, S. Weisser, A. Schönfelder, J. Fleissner, W. Jantz, J. Rosenzweig, and J.D. Ralston, "Improved Performance from Pseudomorphic In_yGa_{1-y}As/GaAs MQW Lasers with Low Growth Temperature Al_xGa_{1-x}As Short-Period Superlattice Cladding," *IEEE Photon. Technol. Lett.*, vol. 7, pp. 16-18, 1995.
- ² J.D. Ralston, E.C. Larkins, W. Rothmund, I. Esquivias, S. Weisser, J. Rosenzweig, and J. Fleissner, "Enhancements in MBE-Grown High Speed GaAs and In_{0.35}Ga_{0.65}As MQW Laser Structures Using Binary Short-Period Superlattices," 7th International Conference on Molecular-Beam Epitaxy, Schwäbisch Gmünd, Germany, August 1992.
- ³ S. Weisser, C. Larkins, K. Czotscher, W. Benz, J. Daleiden, I. Esquivias, J. Fleissner, J. D. Ralston, B. Romero, R. E. Sah, A. Schönfelder and J. Rosenzweig, "Damping-Limited Modulation Bandwidths Up to 40 GHz in Undoped Short-Cavity In_{0.35}Ga_{0.65}As-GaAs Multiple-Quantum-Well Lasers", *IEEE Photon. Tech. Lett.*, vol. 8, n. 5, pp. 608-610, 1996
- ⁴ M. Hagberg, A. Larsson, and S. T. Eng, "Single-ended output GaAs/AlGaAs single quantum well lasers with a dry-etched corner reflector," *Appl. Phys. Lett.*, vol. 56, pp. 1934-1936, 1990.
- ⁵ S. D. Smith, J. L. Fitz, and J. K. Whisnant, "CW Operation of Corner Cavity Semiconductor Lasers," *IEEE Photon. Technol. Lett.*, vol. 5, pp. 876-878, 1993.
- ⁶ G. M. Smith, D. V. Forbes, J. J. Coleman, and J. T. Verdeyen, "Optical Properties of Reactive Ion Etched Corner Reflector Strained-Layer InGaAs-GaAs-AlGaAs Quantum-Well Lasers," *IEEE Photon. Technol. Lett.*, vol. 5, pp. 873-876, 1993.
- ⁷ Z. J. Fang, G. M. Smith, D. V. Forbes, and J. J. Coleman, "A Corner Reflector InGaAs-GaAs Strained Layer Single Quantum Well Coupled Laser Array," *IEEE Photon. Technol. Lett.*, vol. 6, pp. 10-12, 1994.
- ⁸ I.P. Kaminow and R.S. Tucker, "Mode-Controlled Semiconductor Lasers," Chapter 5 in *Guided-Wave Optoelectronics*, ed. by T. Tamir, Springer-Verlag, Berlin, 1990.
- ⁹ P.A. Morton, T. Tanbun-Ek, R.A. Logan, A.M. Sergent, P.F. Sciortino, Jr., and D.L. Coblenz, "Frequency Response Subtraction for Simple Measurement of Intrinsic Laser Dynamic Properties," *IEEE Photon. Technol. Lett.*, vol. 4, pp. 133-136, 1992.
- ¹⁰ L.F. Lester, "High Frequency Multiple Quantum Well Strained-Layer Lasers," Ph.D. dissertation, Cornell University, Ithaca, NY, 1992.
- ¹¹ S. Weisser, personal communication, Fraunhofer-Institut für Angewandte Festkörperphysik, Freiburg, Germany.
- ¹² A. Cremades and J. Piqueras, "Luminescence study of structural changes induced by laser cutting in diamond films," *J. Appl. Phys.*, vol. 78, pp. 3353-3356, 1995.
- ¹³ Research Devices Model M-8a Flip Chip Aligner Bonder, Research Devices, Inc., 121 Ethel Rd. West, Piscataway, NJ 08854.

-
- ¹⁴ G.P. Agrawal and N.K. Dutta, *Long-Wavelength Semiconductor Lasers*, Van Nostrand Reinhold, New York, NY, 1986.
- ¹⁵ D. A. Ackerman, G. E. Shtengel, M. S. Hybertsen, P. A. Morton, R. F. Kazarinov, T. Tanbun-Ek, and R. A. Logan, "Analysis of Gain in Determining T_0 in 1.3 μm Semiconductor Lasers", *IEEE J. of Select. Topics in Quant. Electron.*, vol. 1, n. 2, pp. 250-263, 1995
- ¹⁶ T. Uchida, H. Kurakake, H. Soda, and S. Yamazaki, "CW Operation of a 1.3- μm Strained Quantum Well Laser on a Graded InGaAs Buffer with a GaAs Substrate", *1995 IEEE 7th International Conference on Indium Phosphide and Related Materials*, IEEE, New Jersey, pp. 22-25, 1995
- ¹⁷ M. Peter, K. Winkler, M. Maier, N. Herres, J. Wagner, D. Fekete, K. H. Bachem, and D. Richards, "Realization and modeling of a pseudomorphic $(\text{GaAs}_{1-x}\text{Sb}_x\text{-In}_y\text{Ga}_{1-y}\text{As})/\text{GaAs}$ bilayer-quantum well", *Appl. Phys. Lett.*, vol. 67, n. 18, pp. 2639-2641, 1995
- ¹⁸ S.-H. Wei, D. B. Laks, A. Zunger, Dependence of the Optical Properties of Semiconductor Alloys on the Degree of Long-Range Order", *Appl. Phys. Lett.*, vol. 62, n. 16, pp. 1937-1939, 1993
- ¹⁹ T. Hayakawa, K. Takahashi, T. Suyama, M. Kondo, S. Yamamoto, and T. Hijikata, "Enhancement of Heavy-Hole-Related Excitonic Optical Transitions in (111)-Oriented Quantum Wells", *Jap. J. of Appl. Phys., Pt. 2*, vol. 27, n. 3, pp. L300-L303, 1988
and T. Hayakawa, M. Kondo, T. Suyama, K. Takahashi, S. Yamamoto, and T. Hijikata, "Enhancement of the Capture Rate of Carriers in (111)-Oriented GaAs/AlGaAs Quantum Well Structures", *Jap. J. of Appl. Phys. Pt. 2*, vol. 27, n. 5, pp. L762-L765, 1988
- ²⁰ T. Ohtoshi, T. Kuroda, A. Niwa, and S. Tsuji, "Dependence of Linewidth Enhancement Factor on Crystal Orientation in Strained Quantum Well Lasers", *IEEE Photon. Tech. Lett.*, vol. 6, n. 12, pp. 1424-1426, 1994
- ²¹ A. Schönfelder, S. Weissner, I. Esquivias, J.D. Ralston, and J. Rosenzweig, "Theoretical Investigation of Gain Enhancements in Strained $\text{In}_{0.35}\text{Ga}_{0.65}\text{As}/\text{GaAs}$ MQW Lasers via p-Doping", *IEEE Photon. Technol. Lett.*, vol. 6, pp. 475-477, 1994.

MISSION OF ROME LABORATORY

Mission. The mission of Rome Laboratory is to advance the science and technologies of command, control, communications and intelligence and to transition them into systems to meet customer needs. To achieve this, Rome Lab:

- a. Conducts vigorous research, development and test programs in all applicable technologies;
- b. Transitions technology to current and future systems to improve operational capability, readiness, and supportability;
- c. Provides a full range of technical support to Air Force Material Command product centers and other Air Force organizations;
- d. Promotes transfer of technology to the private sector;
- e. Maintains leading edge technological expertise in the areas of surveillance, communications, command and control, intelligence, reliability science, electro-magnetic technology, photonics, signal processing, and computational science.

The thrust areas of technical competence include: Surveillance, Communications, Command and Control, Intelligence, Signal Processing, Computer Science and Technology, Electromagnetic Technology, Photonics and Reliability Sciences.